International Journal of Nanomedicine

Dovepress
Taylor & Francis Group

Open Access Full Text Article

ORIGINAL RESEARCH

ROS/pH Dual-Responsive Hydrogel Dressings Loaded with Amphiphilic Structured Nano Micelles for the Repair of Infected Wounds

Jun Wang[1,*], Yanxia Lin[1,2,*], Huijing Fan[1], Jianfeng Cui[1], Yuanxiang Wang[1], Zilan Wang[1]

[1]The Department of Rehabilitation Medicine, Shenzhen Qianhai Shekou Free Trade Zone Hospital, Shenzhen, 518067, People's Republic of China; [2]Guangzhou Myers Biotechnology Co., Ltd, Guangzhou, 510660, People's Republic of China

*These authors contributed equally to this work

Correspondence: Yanxia Lin; Jun Wang, The Department of Rehabilitation Medicine, Shenzhen Qianhai Shekou Free Trade Zone Hospital, No. 128, 7th Road, Shekou Industrial Zone, Shenzhen, Guangdong, 518067, People's Republic of China, Email 540147960@qq.com; wangjun0743@163.com

Background: Bacterial infections in wounds have emerged as an increasingly significant healthcare concern. The toxins secreted by bacteria cause persistent inflammation and excessive oxidative stress, resulting in serious tissue damage and ultimately delay wound healing.

Methods: Herein, a ROS/pH dual-responsive hydrogel dressing loaded with amphiphilic structured nano micelles was developed for efficiently promoting infected wound healing. First, chitosan-grafted α-lipoic acid (CSLA) and curcumin (Cur) formed stable amphiphilic nano micelles (CSLA@Cur) through ultrasonic self-assembly. Subsequently, CSLA@Cur was incorporated into a hydrogel formed from 4-carboxyphenylboronic acid-modified gelatin methacrylate (GelMA-CPBA) and oxidized chondroitin sulfate (OCS) via Schiff base formation, boronate ester bonding, and free radical polymerization to obtain GC/OCS-CL@Cur hydrogel dressing. The mechanical properties, antimicrobial, antioxidant, and ROS/pH responsiveness of GC/OCS-CL@Cur were evaluated. Cellular assays were performed to investigate the biocompatibility of GC/OCS-CL@Cur and its role in promoting angiogenesis, scavenging intracellular ROS and regulating macrophage polarization. A full-thickness skin defect rat model with bacterial infection was established to investigate the ability of GC/OCS-CL@Cur to enhance wound repair in vivo.

Results: The unique cross-linked structure of GC/OCS-CL@Cur significantly improves the mechanical properties of hydrogels. Importantly, GC/OCS-CL@Cur exhibited sensitive ROS/pH dual responsiveness, which enabled the controlled release of CSLA@Cur and efficient delivery of Cur. Moreover, GC/OCS-CL@Cur possessed excellent antimicrobial activity and efficient ROS scavenging ability. In vitro cellular assays demonstrated that GC/OCS-CL@Cur could effectively scavenge intracellular ROS (up to 90% scavenging ratio), promote macrophage polarization to M2 phenotype, and enhance angiogenesis. In vivo experiments showed that GC/OCS-CL@Cur significantly regulated the expression level of inflammatory cytokines, and healed more than 95% of wounds in 14 days, showing excellent wound healing ability.

Conclusion: These results demonstrate the successful development of a dual-responsive (ROS/pH) hydrogel dressing with integrated antibacterial, antioxidant, and anti-inflammatory properties, showcasing significant potential for treating infected wounds.

Keywords: nano micelles, microenvironment response, antioxidant, anti-inflammatory, infected wound

Introduction

The skin, the largest organ in the human body, serves a number of purposes, such as preventing injury to internal organs and maintaining their warmth and moisture content.[1] Nonetheless, the integument is remarkably susceptible to trauma. In the event of injury, the wound is vulnerable to bacterial infection, which can lead to significant oxidative stress and inflammatory reactions. These reactions, in turn, can result in substantial tissue damage and vascularization dysfunction, consequently delaying the healing process.[2] Therefore, eliminating bacterial infection, reducing oxidative stress and inhibiting inflammatory response are important components of the wound healing process. These elements collectively

Received: 13 February 2025
Accepted: 13 June 2025
Published: 23 June 2025

promote the formation of new blood vessels.[3] However, it is challenging to effectively promote wound healing over the long term due to the drawbacks of traditional wound dressings (such as gauze, band-aids, etc)., which include poor antibacterial performance, insufficient biological activity, and an inability to provide a suitable moist environment.[4,5] The creation of novel hydrogel wound dressings that resemble natural extracellular matrix and have a variety of biological activities has recently drawn a lot of interest for the treatment of wound healing.

Compared with traditional wound dressings, natural polymer hydrogel dressings (such as alginate, hyaluronic acid, gelatin (Gel), chondroitin sulfate (CS), etc). have excellent biocompatibility and degradability, and can reduce adverse reactions such as allergies.[6–8] The hydrogel's ability to adhere to the wound surface serves as a physical barrier, hindering bacterial infiltration and contributing to the wound's healing process. The hydrogel's high moisturizing properties contribute to the maintenance of a moist environment, which is conducive to wound healing and is a key condition for cell regeneration.[9] Recently, a variety of hydrogels with diverse applications have been developed, including injectable, self-healing, and microenvironmentally responsive properties.[10] Among them, microenvironment-responsive hydrogels, which can adjust their properties and functions under different conditions by responding to the microenvironment (such as reactive oxygen species (ROS), pH), have received a lot of attention in biomedical applications.[11] Studies have shown that hydrogels based on boronate ester bonds can achieve a sensitive response to ROS because the boron atoms of borate bonds have empty p orbitals, which makes it easy to react with hydrogen peroxide. When hydrogen peroxide attacks the boron atom, a reaction similar to the Baeyer-Villiger oxidative rearrangement occurs, followed by hydrolysis, which eventually breaks the link.[12] In addition, hydrogels based on Schiff base bonds will undergo hydrolytic fracture of bonds under low pH conditions, thus achieving pH responsiveness and promoting the degradation of hydrogels.[13] The utilization of microenvironment-responsive hydrogels in the delivery of drugs offers numerous advantages, including the capacity for controlled release and enhanced targeting.[14] Qiao et al[15] developed a series of ROS-responsive hydrogels crosslinked via boronate ester bonds between hyaluronic acid-grafted 3-aminophenylboronic acid (HA-PBA) and poly(vinyl alcohol) (PVA) for wound repair. These hydrogels were designed to facilitate the controlled delivery of anti-inflammatory drugs. Xie et al[16] developed a pH-responsive drug-releasing microcarrier composite hydrogel that releases vascular endothelial growth factor (VEGF) and promotes angiogenesis in response to changes in pH, thereby effectively facilitating the repair of bacterial infected wounds. In order to treat skin wound healing, He et al[17] developed a multifunctional ROS/pH dual-responsive hydrogel for loading and slowing the release of platelet-rich plasma (PRP) made from human cord blood to promote wound healing. Drug loading simultaneously gives the hydrogel a variety of biological characteristics, including anti-inflammatory and antioxidant benefits. Because of these characteristics, hydrogels can actively aid in the healing of damaged tissue.[18]

Curcumin (Cur) exhibits substantial anti-inflammatory and antioxidant properties, thereby establishing it as a pivotal component for wound healing.[19] However, due to its water insolubility, its application in biomedicine is limited.[20] Nano-borne drug systems have emerged as a dynamic, effective, and promising strategy in the treatment of various diseases. The remarkable structural stability and degradability of amphiphilic nano micelles make them highly promising for drug delivery.[21] The hydrophobic core inside the micelle can effectively wrap hydrophobic drugs and prevent the premature release of drugs, while the hydrophilic part is oriented towards the aqueous solution and maintains its high-water solubility, thus forming a stable core-shell nanostructure.[22] A micellar hydrogel platform containing rifampicin and curcumin was created by Zhao et al[23] to treat bacterial infections in chronic wounds. The micelles that were loaded with curcumin and rifampicin have been shown to exhibit a response to MMP9 and an ability to target epidermal growth factor receptor (EGFR). A highly selective dual-responsive hydrogel with low pH and high ROS was created by Hu et al[24] by grafting phenyl boric acid onto the side chain of an alginate polymer. The intelligent hydrogel was then loaded with micelles containing the antibiotic Amikacin (AM) and the anti-inflammatory medication naproxen (Nap), creating a unique drug delivery system intended to promote the healing of infected wounds. α-Lipoic acid (ALA) is an amphiphilic compound with excellent antioxidant activity (containing hydrophilic carboxyl groups and hydrophobic 1, 2-disulfide heterocyclopentane). Because it contains multiple auto polymeric reaction sites, it is easy to functionalize modification, which makes ALA-based nano micelles have great potential in the application of wound healing.[25,26] Yuan et al[27] developed a series of amphiphilic low-molecular-weight chitosan-lipoic acid (LC-LA) conjugates with tunable LA

substitution degrees using N,N′-carbonyl diimidazole (CDI) as the catalyst. These conjugates self-assembled into redox-responsive micelles exhibiting high doxorubicin (Dox) loading capacity.

In this study, ROS/pH dual-responsive hydrogel dressings loaded with amphiphilic structured nano micelles were designed to promote the healing of infected wounds. First, chitosan was grafted to the hydrophilic end of ALA at room temperature. Then, stable amphiphilic drug-carrying nano micelles (CSLA@Cur) were prepared by ultrasonic self-assembly after adding Cur into a chitosan-grafted ALA polymer (CSLA) solution (Figure 1a). Subsequently, oxidized chondroitin sulfate (OCS) was formed by oxidizing CS by sodium periodate (Figure 1b). Gel was modified using methacrylic anhydride (MA) and 4-carboxyphenylboronic acid (CPBA) to obtain GelMA-CPBA (Figure 1c). Finally, GelMA-CPBA and OCS formed a composite hydrogel (GC/OCS) through Schiff base formation, boronate ester bonding,

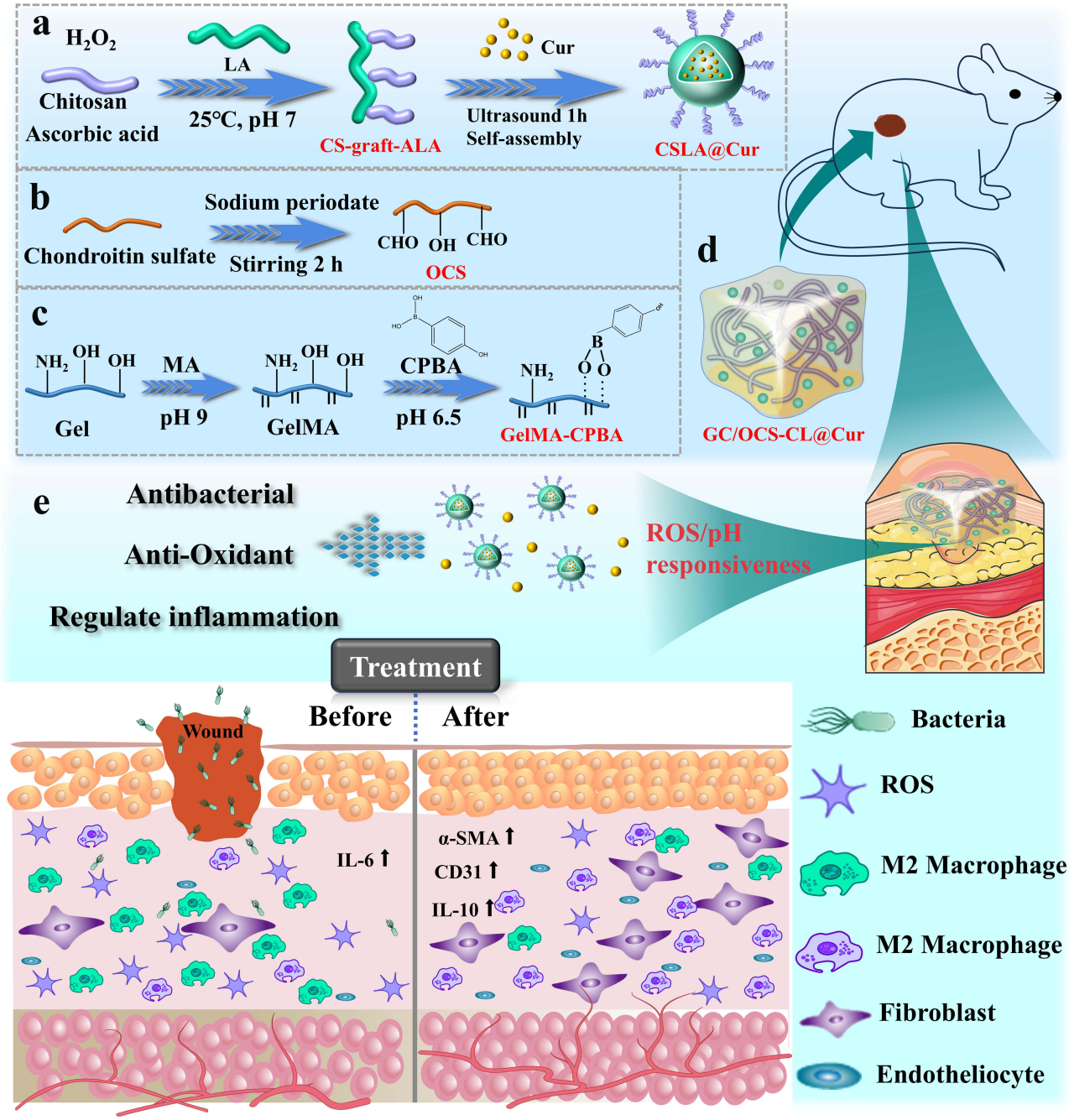

Figure 1 The preparation process of GC/OCS-CL@Cur and the mechanism in promoting the healing of bacterial infection wounds.

https://doi.org/10.2147/IJN.S522589

and free radical polymerization. Before gelling, CSLA@Cur was wrapped inside to form a GC/OCS-CL@Cur hydrogel dressing (Figure 1d). The unique cross-linked structure of GC/OCS-CL@Cur enhances the mechanical properties of the hydrogel and provides excellent wettability for wound healing. In addition, due to the presence of boronate ester and Schiff base bonds, GC/OCS-CL@Cur can respond to the high ROS and low pH microenvironment of the wound, thereby releasing the nano micelles (CSLA@Cur). CSLA@Cur possesses excellent antimicrobial and antioxidant activities and is able to exert sustained anti-inflammatory effects through the slow release of Cur (Figure 1e). These properties endow GC/OCS-CL@Cur with great potential for promoting the healing of infected wounds.

Experimental Methods

Materials

Chitosan (CS, deacetylation ≥95%, MW 50,000–60,000), ascorbic acid (≥99.0%), hydrogen peroxide (7.7 wt. % in H_2O), α-lipoic acid (ALA, 99%), sodium hydroxide (95%, granular) and 2-Hydroxy-4′- (2-hydroxyethyl)-2-methylpropiophenone (I2959, 98.00%) were sourced from Shanghai Maclin Biochemical Technology Co., LTD. Curcumin (Cur, 98%), Chondroitin sulfate (CS, 97%), sodium periodate (99.5%), gelatin (BR grade), sodium carbonate-sodium bicarbonate, 4-carboxyphenylboric acid (CPBA, 99%), methacrylate anhydride (MA, 94%), 1-(3-Dimethylaminopropyl)-3-ethylcarbodiimide (EDC, 99.5%) and N-Hydroxy succinimide (NHS, 99%) were derived from Shanghai Titan Technology Co., LTD.

Preparation of CSLA and CSLA@Cur

Firstly, CSLA and CSLA@Cur (for short, CL@Cur) nano micelles were prepared by ultrasonic technology using the method of Shen et al.[28] In 90.00 mL of 2% acetic acid aqueous solution, dissolve 1.00 g of chitosan. Using ascorbic acid 0.10 g and hydrogen peroxide 1.30 mL (7.7%) as catalysts, the mixture was stirred at room temperature for 30 min. After a 24-hour reaction at ambient temperature, 0.25 g of ALA ethanol solution is meticulously introduced to the mixture. Subsequently, sodium hydroxide is employed to adjust the pH of the resultant solution to a neutral state. The CSLA polymer was subsequently obtained through a freeze-drying process on the residual fluid following the elimination of the precipitate by centrifugation after a 3-d period of dialysis in pure water. The CSLA polymer was dissolved in a sterile water solution to yield a concentration of 1.00 mg/mL. Subsequently, the resultant aqueous solution of the polymer was subjected to ultrasonic treatment with an amplitude of 40 (750 W, 20 kHz) for a duration of 1 h. This treatment was carried out using a VCX 750 probe ultrasonic instrument, to produce the CSLA nano micelles. Fourier transform infrared spectrometer (FTIR, ZEISS sigma500) and ^{1}H nuclear magnetic resonance spectra (^{1}H NMR, AVANCE III HD 400M) tests on CS and CSLA were performed to demonstrate successful grafting of CS on ALA.

To ensure complete encapsulation, 0.10 mg/mL (C_0) of curcumin solution (dissolved in a methanol solution) was added to the micellar solution, and a 1 h room-temperature ultrasonography was conducted. Finally, the mixture was evaporated by rotation at 37 °C to remove the methanol and filtered by 0.45 μm filter membrane to remove the unencapsulated Cur. An ultraviolet spectrophotometer was used to measure the filtrate's absorbance at 426 nm, and formula (1) was used to determine the concentration of successfully encapsulated curcumin (C_1). Finally, it was freeze-dried to obtain CSLA@Cur and stored at 4 °C. The internal morphology and particle size distribution of CSLA and CSLA@Cur were tested using a transmission electron microscope (TEM, JEM 2100 F) and a liquid Zeta particle size analyzer (Zetasizer Nano S90).

$$\text{Cur loading}\,(\text{mg/g}) = \frac{(C_0 - C_1) \times V}{m} \tag{1}$$

Where, C_0 (mg/mL) is the initial addition concentration of the Cur, C_1 (mg/mL) is the concentration of the Cur that was not successfully encapsulated, and V (mL) is the solution volume, m (g) is the mass of CSLA@Cur.

Preparation of OCS, GelMA-CPBA and GC/OCS

Then, GC/OCS hydrogels were prepared concerning the study of Zhou et al.[29]

First, dissolve 1.00 g chondroitin sulfate in 100.00 mL deionized water, while dissolving 0.27 g sodium periodate in 5.00 mL deionized water. Subsequently, the two solutions were amalgamated and agitated in the absence of light at ambient temperature at 600 rpm for a period of 2 h. Thereafter, 1.00 mL of glycol was introduced into the mixture to affect the termination of the reaction and the consequent formation of OCS. The CS and OCS were tested using FTIR (ZEISS sigma500) and ^{1}H NMR (AVANCE III HD 400M) to confirm the successful synthesis of OCS.

Then, Gel (10.00 g) was added to the sodium carbonate-sodium bicarbonate solution (100.00 mL) and stirred at 50 °C until completely dissolved. The pH of the liquid was then lowered to 9.0 by adding drops of methacrylate anhydride (0.38 mL) and a sodium hydroxide solution (1.00 mol/L). After three hours, the reaction was neutralized using hydrochloric acid (1.00 mol/L). The mixture was dialyzed with deionized water for 5 d and then freeze-dried for 3 d to produce GelMA. Subsequently, GelMA (0.50 g) is introduced into 25.00 mL of water at 37 °C, where it is agitated until complete dissolution occurs. Subsequently, EDC (1.00 mmol), CPBA (1.00 mmol), and NHS (1.00 mmol) were added sequentially to the DMF (9.00 mL) and water (6.00 mL) mixture. After that, the combination was left to react at room temperature for 30 min Subsequently, droplets of the CPBA solution were added to the GelMA solution, and the pH was elevated to 6.5 with the assistance of the NaOH solution. To obtain GelMA-CPBA, the solution underwent dialysis with deionized water for 5 d. Following this, the solution was subjected to freeze-drying after a 24-hour reaction at room temperature. Gel, GelMA and GelMA-CPBA were tested using FTIR (ZEISS sigma500) and ^{1}H NMR (AVANCE III HD 400M) to confirm the successful synthesis of GelMA-CPBA. In addition, a scanning electron microscope (SEM, ZEISS sigma500) was used to analyze the morphology of GelMA-CPBA.

Finally, mix the prepared OCS and GelMA-CPBA in water, and after stirring at room temperature for a certain time, the GC/OCS hydrogel is finally formed. The morphology of GC/OCS was analyzed by SEM (ZEISS sigma500).

Preparation of GC/OCS-CL@Cur

GelMA-CPBA (10.00 wt.%), OCS (2.00 wt.%), I2959 (0.25 wt. %), and CSLA@Cur (0.40 wt. %) were dissolved in water and evenly mixed. Subsequent to being left at room temperature for a period of 3 min, the hydrogel was formed and then cured by ultraviolet (UV, L5S, INESA) for a duration of 5 min. GC/OCS-CL@Cur hydrogel was prepared. The morphology of GC/OCS-CL@Cur was analyzed by SEM (ZEISS sigma500).

Characterization Testing

FTIR spectra were acquired in transmission mode using KBr pellets (1 mg sample per 100 mg KBr), with 16 scans at 4 cm^{-1} resolution over 4000–400 cm^{-1}. ^{1}H NMR spectra were recorded at 600 MHz, using deuterated water (D_2O) as the solvent and tetramethylsilane (TMS) as an internal standard. For TEM, CSLA and CSLA@Cur were dispersed in anhydrous ethanol and dripped onto a carbon-supported membrane copper mesh for observation. For SEM, the hydrogels were liquid nitrogen embrittled and then sprayed with gold to observe the cross sections.

Mechanical Properties of Hydrogels

3 parallel experimental groups were established in each group of GelMA-CPBA, GC/OCS, and GC/OCS-CL@Cur hydrogel, which were molded into a cylinder for the compression test. The test was initiated at a speed of 1.00 mm/min. After the hydrogel sample was compressed to rupture, the compressive stress-strain curve and elastic modulus of the hydrogel were obtained.

The GelMA-CPBA, GC/OCS, and GC/OCS-CL@Cur hydrogel samples were prepared into dumbbell shape (length 30.00 mm, thickness 2.00 mm), and in each group, 3 parallel experimental groups were established. The hydrogel was subjected to a tensile test at a rate of 1.00 mm/min until it broke. The tensile stress-strain curve and elastic modulus of hydrogel were obtained.

Swelling Properties of Hydrogels

Hydrogels GelMA-CPBA, GC/OCS and GC/OCS-CL@Cur were prepared into cylinders for swelling test, and 3 parallel experimental groups were established in each group. Before the swelling test, the hydrogel is weighed first to obtain the initial weight (M_0). After that, the hydrogel is put in an incubator set to 37 °C in a container with phosphate buffered

 https://doi.org/10.2147/IJN.S522589

brine (PBS) buffer. Following a 24-hour period, the hydrogel was taken out and measured to determine its swelling weight (M). Formula (2) was then used to determine the hydrogel's swelling ratio (SR).

$$\mathrm{SR}\,(\%) = \frac{M - M_0}{M_0} \times 100\% \tag{2}$$

Where, M_0 denotes the initial weight of the hydrogel before swelling, while M signifies the weight of the hydrogel after the swelling process.

Drug Release of Hydrogels

A specific amount of GC/OCS-CL@Cur was added to a pH 5.2 PBS solution with abundant H_2O_2 (3 parallel experimental were prepared), and the mixture was then incubated at 37 °C in a shock incubator. Periodically extract a part of the solution (while adding an equal amount of PBS solution), measure its absorbance at 426 nm with an ultraviolet spectrophotometer, and calculate the concentration of the Cur. Finally, the cumulative release ratio (CR) of Cur was calculated and the drug release curve was drawn according to formula (3).

$$\mathrm{CR}\,(\%) = \frac{C_\mathrm{x}}{C_1} \times 100\% \tag{3}$$

Where, C_1 is the concentration of the Cur successfully loaded on CSLA, and C_x is the concentration of the Cur under different drug release times.

Antimicrobial Analysis

Staphylococcus aureus (*S. aureus*) and *Escherichia coli* (*E. coli*) were used as antibacterial specimens, and the absorbance method was used to evaluate the antibacterial properties of different hydrogels. Firstly, the prepared hydrogel samples were placed in the well plate, and the wells without hydrogel were used as blank control groups (3 parallel experimental groups were set up in each group), 100.00 μL bacterial suspension, and 900.00 μL broth were added, and cultured at 37 °C by shock. A bacterial suspension of each sample was collected at different time points and its absorbance was measured at 570 nm using a Biotek Synergy H1 to obtain a bacterial growth curve. In addition, when bacterial growth was observed to be inhibited, 100.00 μL bacterial suspension was extracted and 900.00 μL sterile PBS (pH 7.4) was added for gradient dilution ($\times 10^{-8}$). Subsequently, the diluted bacterial suspension was inoculated onto the solid medium via the coating plate method. The coating plate was subsequently subjected to a culture process within a constant temperature incubator maintained at 37 °C for a duration of approximately 18 h. The growth patterns of the colonies were meticulously observed and documented through photographic records. Finally, the bacterial survival ratio of the material was calculated according to formula (4).

$$\text{Bacterial survival ratio}\,(\%) = \frac{Nx}{N_0} \times 100\% \tag{4}$$

Where, N_0 denotes the number of colonies in the blank control group, while N_x represents the number of colonies in the sample group.

Analysis of Antioxidant Capacity

The 1,1-diphenyl-2-picryl-hydrazyl radical (DPPH) method and the 2,2′-casino-bis (3-ethylbenzothiazoline-6-sulfonic acid) (ABTS) method were used to assess the hydrogels' antioxidant capacity.

DPPH free radical scavenging assay was conducted. First, each group of hydrogels was sterilized by ultraviolet radiation and placed in normal saline (NS) at an extraction ratio of 2 mg/mL for 24 h at 37 °C and 120 rpm to obtain the leaching liquor as the samples to be tested. 3 parallel experimental groups were established in each group, with vitamin C (VC) standard working liquid serving as the positive control group and NS as the blank control group. Then anhydrous ethanol and DPPH solution were added to each set of test tubes. An ultraviolet spectrophotometer (INESA L5S, Shanghai, China) was utilized to ascertain the solution's degree of absorption at 517 nm following a 30-minute reaction at 25 °C. Finally, the DPPH clearance of the positive control group and the sample was calculated according to formula (5) and formula (6).

$$\text{Positive control DPPH clearance}\,(\%) = \frac{A_0 - A_3}{A_0} \times 100\% \tag{5}$$

$$\text{Sample DPPH clearance}\,(\%) = \frac{A_0 - (A_1 - A_2)}{A_0} \times 100\% \tag{6}$$

Where, A_0 is OD_{517nm} of the blank control, A_1 is OD_{517nm} of the sample, A_2 is OD_{517nm} of the sample control, and A_3 is OD_{517nm} of the positive control.

After that, the ABTS method of free radical scavenging was tested. First, each group of hydrogels was sterilized by ultraviolet radiation and placed in NS at an extraction ratio of 2 mg/mL for 24 h at 37 °C and 120 rpm to obtain the leaching liquor as the samples to be tested (3 parallel experimental groups were set up in each group). 0.20 mL extract, blank control sample (NS), and positive control sample (VC standard working liquid) were added to a centrifuge tube containing anhydrous ethanol (0.90 mL) and ABTS reagent (0.90 mL). For 30 min, the mixture is reacted at 25 °C away from light. Subsequently, a UV-Vis spectrophotometer (INESA L5S, Shanghai, China) was employed to ascertain the sample's extinction coefficient at 755 nm. Subsequently, the formulas (7) and (8), which determine the ABTS radical clearance, were employed.

$$\text{Positive control ABTS clearance}\,(\%) = \frac{A_0 - A_3}{A_0} \times 100\% \tag{7}$$

$$\text{Sample ABTS clearance}\,(\%) = \frac{A_0 - (A_1 - A_2)}{A_0} \times 100\% \tag{8}$$

Where, A_0 is OD_{755nm} of the blank control, A_1 is OD_{755nm} of the sample, A_2 is OD_{755nm} of the sample control, and A_3 is OD_{755nm} of the positive control.

In vitro Hemolysis Assay

Hemolysis test: Blood (1.5 mL) was drawn from the orbital venous plexus of mice and diluted with NS (3.5 mL). The erythrocyte suspension (5 mL) was obtained after 5 centrifugal washes (4000 rpm, 5 min). Each group of hydrogels was sterilized by ultraviolet radiation and placed in NS at an extraction ratio of 2 mg/mL for 24 h at 37 °C and 120 rpm to obtain the leaching liquor as the samples to be tested (3 parallel experimental groups were set up in each group). Then, 100.00 μL of erythrocyte suspension was combined with 900.00 μL of leaching liquor. NS was used as negative control group, and deionized water, which is a hypotonic solution that will lead to complete hemolysis of erythrocytes, was used as positive control group. Following a 2-hour incubation at 37 °C, the sample's upper layer was extracted via a centrifugal process. Finally, a UV spectrophotometer was employed to quantify the sample's UV absorption at 450 nm after the preceding dilution of the sample with regular saline. Formula (9), then, was used to determine the hemolysis ratio.

$$\text{Hemolysis}\,(\%) = \frac{H_1 - H_0}{H_2 - H_0} \times 100\% \tag{9}$$

Where, H_0 for the negative control group, OD_{450nm}, H_1 for the sample group of OD_{450nm}, H_2 is the OD_{450nm} of the positive control group.

In vitro Cell Test

Cytotoxicity Assay

The leaching liquid of GC/OCS, CSLA@Cur, and GC/OCS-CL@Cur hydrogels was evaluated for cell viability using the CCK-8 technique after 1, 3, and 5 days of co-cultivation with L929 cells (Shanghai Honsun Biological Technology Co., Ltd). Cell death staining was used to monitor and document the cells' survival. Additionally, crystal violet staining was used to assess each hydrogel group's impact on the cell proliferation ratio at the 3 d.

Cytoskeleton Staining

The cytoskeletal proteins were fluorescently stained with indocyanine green (ICG) after the L929 cells were co-cultured for three days with the leaching liquid of GC/OCS, CSLA@Cur, and GC/OCS-CL@Cur hydrogels. The nucleus was fluorescently stained with 4′,6-diamidino-2-phenylindole (DAPI) in order to assess the morphology of cell diffusion and expansion. Lastly, confocal fluorescence microscopy was used to view and take pictures of the fluorescence staining results.

Scratch Assay

After the L929 cells were equally distributed throughout the 12-well plate, a scratch was created by drawing a straight line with the 200.00 μL gun head perpendicular to the well plate once the cell fusion rate exceeded 98.00%. After adding fresh medium and the leaching liquid of GC/OCS, CSLA@Cur, and GC/OCS-CL@Cur hydrogels to the well plates, they were incubated for 24 h and 48 h, the scratched regions were examined, and pictures were taken. ImageJ software was used to measure the scratch width and compute the cell mobility.

Transwell Assay

L929 cell suspension and the leaching fluid of GC/OCS, CSLA@Cur, and GC/OCS-CL@Cur hydrogels were introduced to the co-cultivation chamber at a 1:1 ratio. Following a 24 h period, crystal violet staining was used to examine and photograph the cell migration. Finally, the number of cells that migrated was quantitatively measured using Image J.

Tube Formation Assay

Following HUVECs (purchased from Shanghai Zeye Biotechnology Co., Ltd). inoculation onto matrix glue-coated 24-well plates, the leaching fluid of the GC/OCS, CSLA@Cur, and GC/OCS-CL@Cur hydrogels were introduced into separate wells. After 6 h of incubation at 37 °C, the vascular network's growth was inspected under a microscope (DMi, Germany) and documented through photographic capture. Subsequently, ImageJ was employed to conduct a quantitative analysis of the vascular network formation.

In vitro H_2O_2 Clearance Experiment

The murine macrophage RAW264.7 cell (purchased from Shanghai Zeye Biotechnology Co., Ltd). line was exposed to a 100 μM H_2O_2 solution for a period of 6 hours. Thereafter, the cells were co-cultured with the leaching liquor of GC/OCS, CSLA@Cur, and GC/OCS-CL@Cur hydrogels for a duration of 24 h. The levels of intracellular reactive oxygen species (ROS) were then determined by 2′,7′-dichlorodihydrofluorescein diacetate (DCFH-DA) staining, and pictures were taken for later analysis. Lastly, ImageJ software was used to perform a quantitative analysis on the pictures.

Macrophage Polarization Immunofluorescence Staining

RAW264.7 cells were exposed to 100.00 ng/mL lipopolysaccharide (LPS) and 20.00 ng/mL interferon-γ (IFN-γ) for a duration of 24 h. Subsequently, RAW264.7 cells were co-cultured with the leaching liquor of GC/OCS, CSLA@Cur, and GC/OCS-CL@Cur hydrogels for an additional 24 h. Immunofluorescence staining was then performed on the cells to detect iNOS and CD206 expression. Lastly, Image J was used to quantitatively measure the fluorescence intensity of CD206 and iNOS in order to assess how hydrogel affected macrophage polarization.

In vivo Animal Experiment

8-week-old female Sprague-Dawley (SD) rats weighing between 190.00–235.00 g were chosen, and they spent 7 d becoming used to the food and conditions of the experiment. All experiments involving animals were approved by the Experimental Animal Ethics Committee of Guangzhou Myers Biotechnology Co., LTD and carried out in accordance with the National Institutes of Health's guidelines for the care and use of laboratory animals. After that, a bacterial-infected full-layer wound defect model was used to evaluate the in vivo wound healing process. First, the rats' dorsal regions were shaved, anesthetized, and sterilized. A skin sampler was then used to make a full-layer skin wound model

incision in the back that was 15.00 mm in diameter. Bacterial infected wounds were modeled by topically and uniformly applying a mixed solution of *E. coli* and *S. aureus* (100 μL, 1×10^9 CFU/mL) to the wound. The experimental rats were separated into 4 groups: control, GC/OCS, CSLA@Cur, and GC/OCS-CL@Cur. The hydrogel group's wounds received the produced hydrogel treatment, while the control group's wounds received PBS treatment (all procedures were performed following an aseptic approach). Photographs were taken on days 3, 7, 10, and 14 after treatment to observe wound healing. After evaluating the wound area using Image J software, the wound healing ratio (HR) was determined according to formula (10).

$$\mathrm{HR}\,(\%) = \frac{M_0 - M_t}{M_0} \times 100\% \tag{10}$$

Where M_0 is the initial trauma cross-sectional area, M_t is the cross-sectional area of healed wounds at different times in each group.

Furthermore, to assess the impact of hydrogel on wound tissue regeneration, hematoxylin and eosin (H&E) staining and Masson staining were used to the wound-healing tissue on days 7 and 14, respectively, to examine the re-epithelialization and collagen deposition of the wound. Using immunohistochemistry examination of wound healing tissue, the expression of inflammatory factors interleukin-6 (IL-6) and interleukin-10 (IL-10) was examined. Finally, platelet endothelial cell adhesion molecule-1 (CD31) and α-smooth muscle actin (α-SMA) fluorescence labeling analysis was used to assess the impact of hydrogel on inducing angiogenesis.

Statistical Analysis

Data are presented as mean±standard deviation (SD) from at least three independent experiments. Statistical significance (*p<0.05, **p<0.01, ***p<0.001) was determined using GraphPad Prism (ANOVA/Tukey' s test or Student' s t-test).

Results and Discussion

Synthesis and Characterization

GC/OCS-CL@Cur is prepared from GelMA-CPBA, OCS and CSLA@Cur by Schiff base reaction, esterification and free radical polymerization. Therefore, the successful synthesis of GelMA-CPBA, OCS and CSLA was first verified by FTIR (Figure 2a–c) and ^{1}H NMR (Figure 2d–f). As can be seen from the FTIR spectrum of GelMA-CPBA (Figure 2a), the intensity of the characteristic peaks in amide band I (C=O stretching vibration) and amide band II (N-H deformation vibration) of GelMA is obviously enhanced compared with that of Gel, which indicates that the methacrylatation of Gel is successful.[30,31] The intensity of the infrared characteristic absorption peaks of OCS at 2929 cm^{-1} and 3336 cm^{-1} is significantly enhanced, which belongs to the O-H stretching vibration and hydroxyl stretching vibration of carboxyl group,[32] respectively (Figure 2b). This phenomenon may be due to the introduction of carboxyl and hydroxyl groups during the oxidation of CS by sodium periodate. This indicates the successful synthesis of OCS. In contrast to the FTIR spectrum of CS, the CSLA spectrum exhibits a new absorption peak at 609 cm^{-1}, which can be attributed to the stretching and bending vibrations of C-H in -CH_2, as shown in Figure 2c. In addition, higher absorption peaks associated with C=O stretching and N-H bending are observed at 1645 cm^{-1} and 1550 cm^{-1} due to the creation of NH-CO groups.[33] This indicated that CS was successfully grafted onto ALA.[28] It can be seen from ^{1}H NMR of GelMA-CPBA (Figure 2d) that the peaks at 5.66 ppm and 5.42 ppm belong to the characteristic peaks of C=C, which indicates that the double-bond modified Gel has been successfully synthesized. The peak at 8.61 ppm belongs to the characteristic peak of the proton in the borate ester bond, indicating the successful synthesis of GelMA-CPBA. The ^{1}H NMR spectra of OCS showed a characteristic peak of aldehyde group at 8.45 ppm, indicating that CS was successfully oxidized by sodium periodate (Figure 2e). In addition, ^{1}H NMR spectra of CSLA showed a new peak at 2.27 ppm, indicating the presence of methylene and methylene protons in the ALA side chain (Figure 2f). This finding confirmed the effective grafting of CS and ALA, thus validating the experimental procedures.[29]

Firstly, CSLA and CSLA@Cur nano micelles were prepared. As illustrated in Figure 2g, the TEM image reveals that the CSLA nano micelles exhibit a well-dispersed, spherical morphology. When CSLA was loaded with Cur, the micellar particles became larger, but they were still uniform nanospheres. Following that, the hydration particle size test analysis

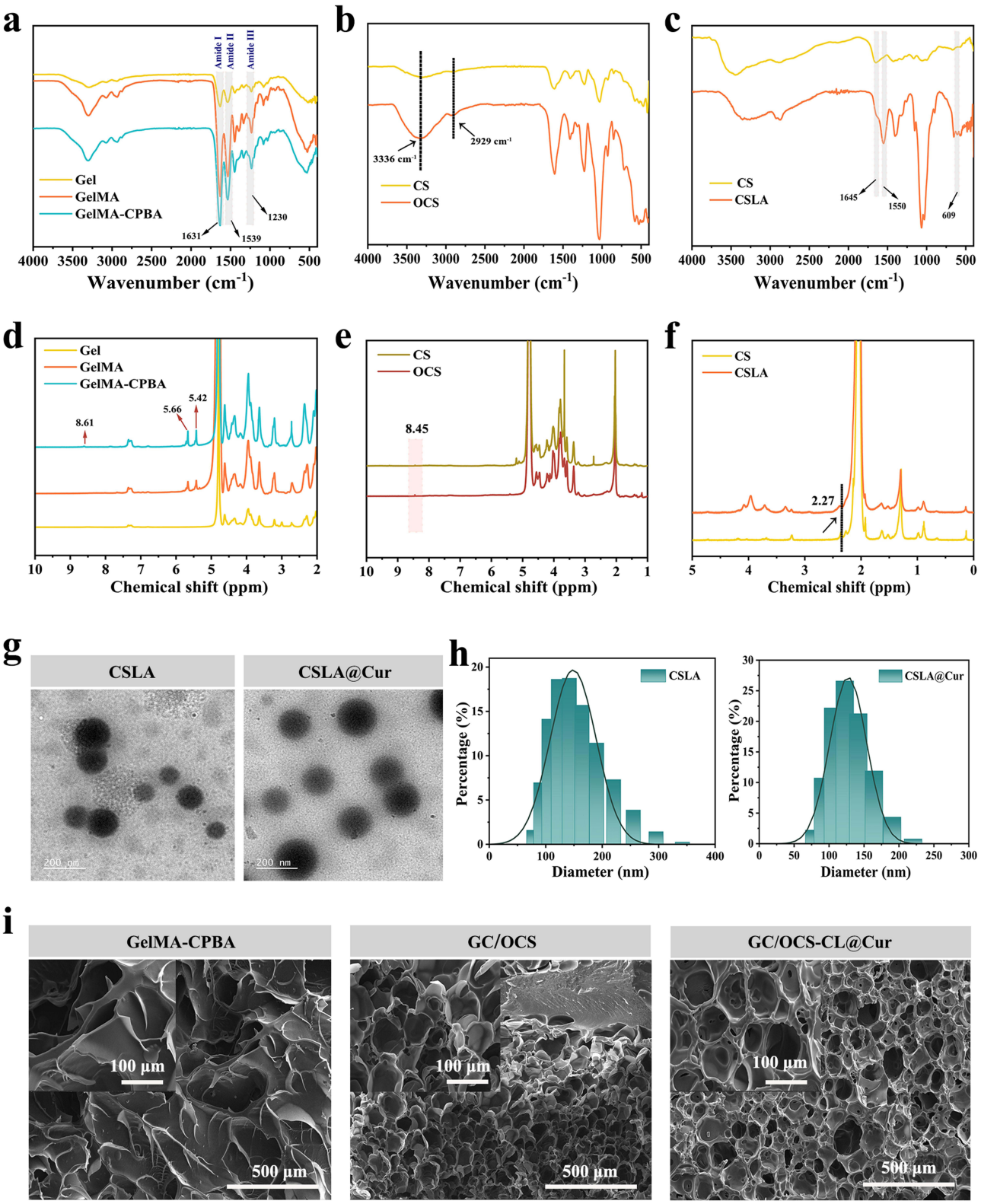

Figure 2 FTIR analysis of (**a**) GelMA-CPBA, (**b**) OCS, and (**c**) CSLA and its components. ^{1}H NMR spectra of (**d**) GelMA-CPBA, (**e**)OCS, and (**f**) CSLA and its components. (**g**) TEM images and (**h**) particle size distribution curves of CSLA and CSLA@Cur. (**i**) SEM images from GelMA-CPBA, GC/OCS, and GC/OCS-CL@Cur.

of CSLA and CSLA@Cur micro micelles yielded the following results (Figure 2h): the average particle size of CSLA is 165.8 nm, with the distribution of particle sizes falling between 78.82 and 341.99 nm. The average particle size of CSLA@Cur is 173.5 nm, with a range of 78.82 to 220.19 nm. This shows that the particle size increases and becomes more uniform after CSLA loading, which is consistent with TEM analysis results. Then, GelMA-CPBA, GC/OCS, and GC/OCS-CL@Cur hydrogels were prepared, and their surface morphologies were analyzed by SEM (Figure 2i). GelMA-CPBA hydrogel presents a network structure with thick pore walls and few pore walls. When -NH_2 on GelMA-CPBA and -CHO on OCS were formed by Schiff base reaction to form GC/OCS composite hydrogels, the network structure of the composite hydrogels became dense and uniform, but the inner wall was jagged. Finally, by introducing CSLA@Cur nano micelles into the composite hydrogel, the network structure of the GC/OCS-CL@Cur hydrogel is arranged regularly, and the pore walls are smooth and flat.

Mechanical Properties, Swelling Properties, and Drug Release Behavior of GC/OCS-CL@Cur

The mechanical properties of hydrogels are such that they can effectively protect wounds from external mechanical damage,[34] to effectively promote the healing of the wound. A series of mechanical tests were conducted on GelMA-CPBA, GC/OCS, and GC/OCS-CL@Cur hydrogels to assess their mechanical properties. Figure 3a shows the compressive stress-strain curves of GelMA-CPBA, GC/OCS, and GC/OCS-CL@Cur. The figure illustrates that the compression ratio of GelMA-CPBA, GC/OCS, and GC/OCS-CL@Cur hydrogels showed a trend of gradual increase, all of which exceeded 50% compression ratio. Among them, the compression ratio of GC/OCS-CL@Cur is 72.03%, but its compressive elastic modulus is only 28.86 kPa, while that of GC/OCS is 44.44 kPa (Figure 3b and c). In addition, the elongation of GelMA-CPBA, GC/OCS, and GC/OCS-CL@Cur hydrogels gradually increased. The elongation of GelMA-CPBA hydrogel was 82.82% and the breaking strength was 13.34 kPa, while the elongation and breaking strength of GC/OCS hydrogel were increased to 102.41% and 36.20 kPa, respectively. The results of this investigation suggest that adding OCS to GelMA-CPBA hydrogels could significantly improve the materials' tensile characteristics (Figure 3d and e). In addition, although the elongation of GC/OCS-CL@Cur hydrogel is increased by 22.56% compared with GC/OCS, the elastic modulus of GC/OCS-CL@Cur hydrogel is decreased from 32.70 kPa to 22.57 kPa. This indicates that the introduction of CL@Cur reduces the stiffness of the hydrogel and makes it more flexible (Figure 3f).

The swelling properties of hydrogels play an instrumental role in the field of drug delivery systems. The capacity for substantial swelling facilitates the absorption of wound exudate and metabolic substances, as well as the diffusion and release of drugs.[35] Therefore, swelling experiments were carried out on GelMA-CPBA, GC/OCS, and GC/OCS-CL@Cur hydrogels and the results are shown in Figure 3g. After GelMA-CPBA and OCS were combined, the swelling ratio was reduced by 31.93%. This could be as a result of OCS hydrogels increasing the composite hydrogels' crosslinking density, which lowers the degree of swelling.[36] However, after the introduction of drug-loaded nano micelles CSLA@Cur, the swelling ratio of GC/OCS-CL@Cur increased by 19.54%, which may be because the nano micelles have certain chemical activity, and the number of hydrogel crosslinking points is reduced through the destruction of hydrogen bonds in the hydrogel,[37] thus reducing the crosslinking density of the hydrogel and increasing the swelling property. This suggests that the coating of CSLA@Cur can balance the swelling properties of the hydrogel, which is very conducive to the diffusion and release of the drug.

Subsequently, the drug release behavior of GC/OCS-CL@Cur was investigated in PBS buffers at pH 5.2 and treated with H_2O_2. The pH/ROS responsiveness of GC/OCS-CL@Cur was evaluated by analyzing the Cur release ratio in GC/OCS-CL@Cur. As can be seen from the Cur drug release curve (Figure 3h) and the bar chart of release ratio statistics (Figure 3i), the Cur release ratio of GC/OCS-CL@Cur in pH 5.2 environment (51.55%) was significantly higher than that in pH 7.4 environment (41.34%). This indicates that GC/OCS-CL@Cur can accelerate drug release in an acidic environment and has an excellent pH response. When GC/OCS-CL@Cur was in an environment rich in H_2O_2, the Cur release ratio was slightly increased (57.27%). However, when GC/OCS-CL@Cur was exposed to both acidic and high ROS levels, the Cur release ratio was significantly enhanced, reaching 68.75%, which was 66.30% higher than the drug release ratio under normal physiological conditions. The above results demonstrate the dual responsiveness of GC/

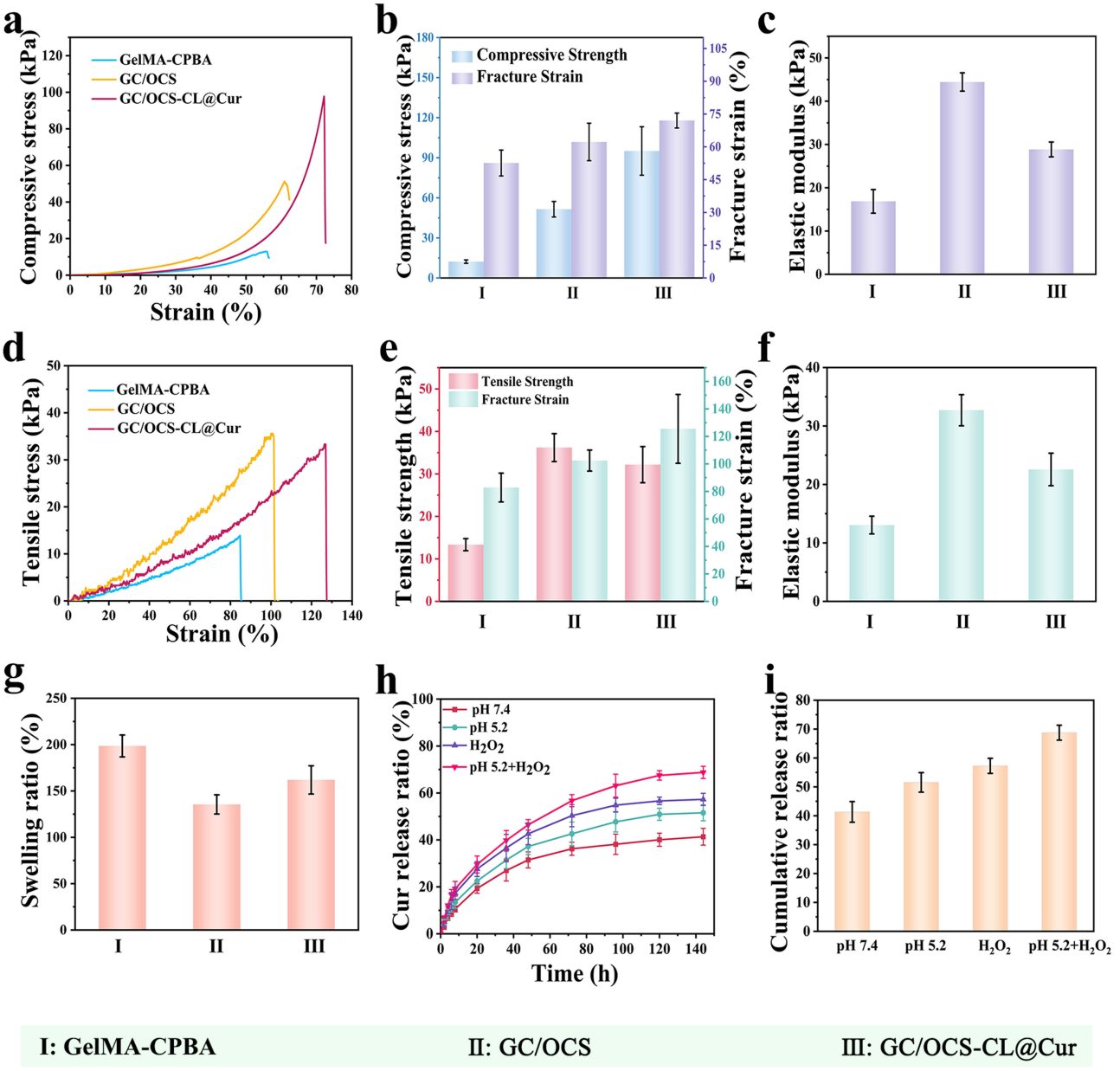

Figure 3 (**a**) compressive stress-strain curve, (**b**) quantitative statistics of compression, and (**c**) elastic modulus of GelMA-CPBA, GC/OCS, and GC/OCS-CL@Cur. GelMA-CPBA, GC/OCS, and GC/OCS-CL@Cur for (**d**) tensile stress-strain curves, (**e**) quantitative statistics of tensile, and (**f**) elastic modulus. (**g**) Swelling ratio of GelMA-CPBA, GC/OCS, and GC/OCS-CL@Cur hydrogels. GC/OCS-CL@Cur (**h**) drug release curves and (**i**) release ratio in response to different microenvironments.

OCS-CL@Cur in the environment of low pH and high ROS levels, which is conducive to the targeted release of drugs, improves the therapeutic effect of drugs, and effectively promotes wound healing.

Antibacterial, Antioxidant, and Blood Compatibility of GC/OCS-CL@Cur

One significant aspect impeding wound healing is bacterial infection. When a wound is infected by bacteria, the bacteria can disrupt the wound environment, producing toxins and enzymes that not only damage healthy cells but may also trigger an excessive inflammatory response that hinders healing.[38] The antibacterial performance of the hydrogels was tested using *S. aureus* and *E. coli* as model organisms. The hydrogel showed significant antibacterial activity after co-culturing with bacteria at 37 °C for 12 hours. At this time, the growth of the colony was observed by the dilution coating method (Figure 4a) and the antibacterial ratio was calculated (Figure 4b). Finally, the growth curves of *S. aureus* and *E. coli* were

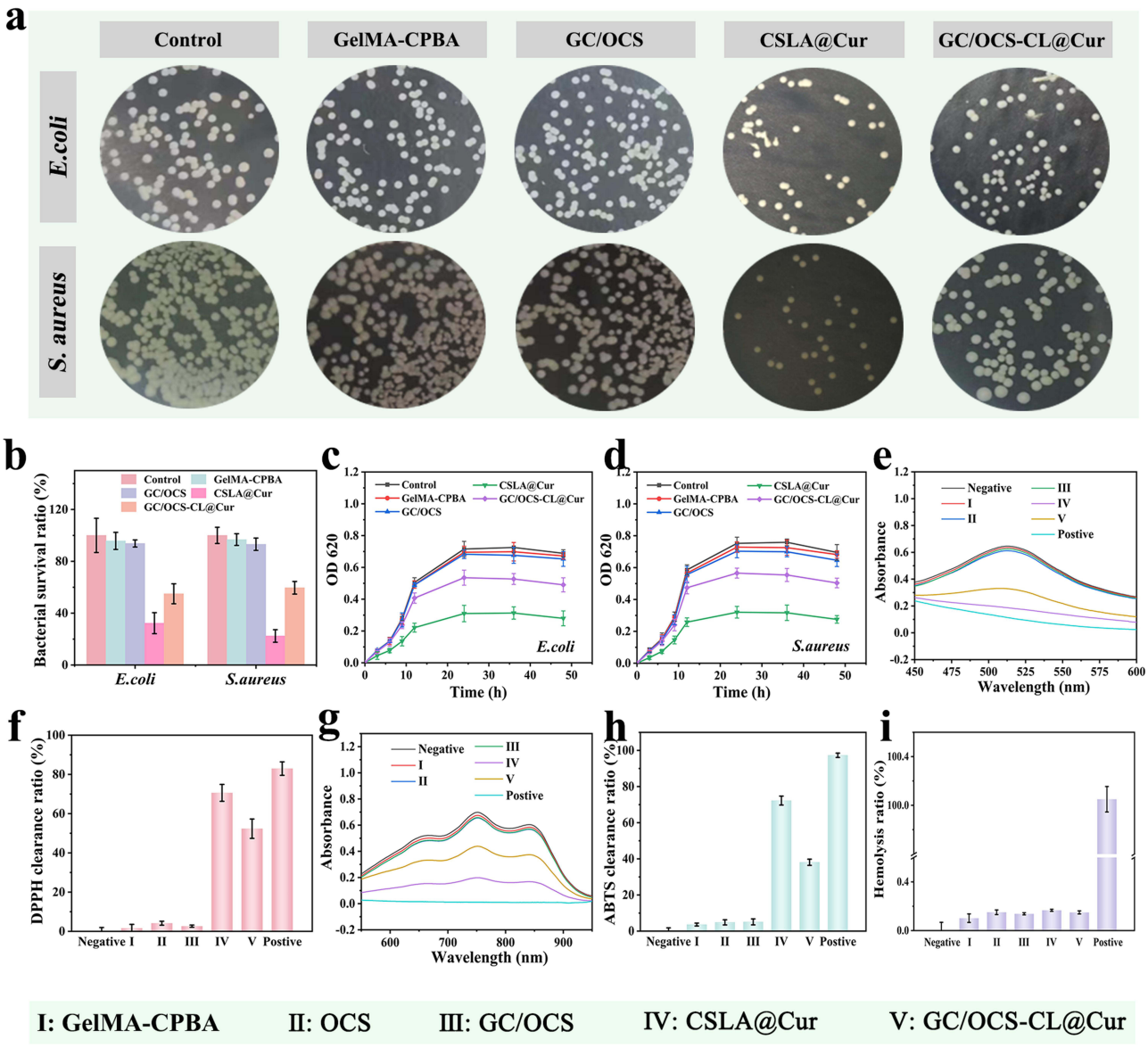

Figure 4 (**a**) Antibacterial coating images of *E. coli* and *S. aureus* by hydrogels and nano micelles, respectively, and (**b**) quantitative statistics of bacterial survival ratio. Growth curves of (**c**) E. coli and (**d**) S. aureus co-cultured with various hydrogels and nano micelles. (**e**) UV absorption spectrum analysis and (**f**) quantitative statistics of DPPH free radical scavenging of hydrogels in each group. (**g**) UV absorption spectrum analysis and (**h**) quantitative statistics of ABTS clearance of hydrogels in each group. (**i**) hemolysis ratio of each hydrogel.

obtained by tracking the bacterial suspension's OD value for 48 h (Figure 4c and d). As the figure shows, the bacteriostatic effect of the GelMA-CPBA, and GC/OCS groups was not significant, while the CSLA@Cur group's *E. coli* and *S. aureus* survival ratios were only 22.39% and 32.03%, respectively. This indicates that CSLA@Cur has excellent antibacterial properties, which may be because CS, as the hydrophilic shell of nano micelles, can fully contact bacteria and destroy the membrane permeability and protein synthesis of bacteria, thus achieving excellent antibacterial effects. The antibacterial effect of CSLA@Cur was somewhat diminished when it was encapsulated in the hydrogel (the bacterial survival ratio of *E. coli* and *S. aureus* was 54.95% and 59%, respectively). This could be because the hydrogel's encapsulation of the nano micelle decreased the area of contact between CS and the bacteria. However, because the hydrogel is responsive to the wound microenvironment, it can intelligently release CSLA@Cur to play an antibacterial role.

The balance between oxidation and antioxidants is crucial for wound healing. Outstanding antioxidant activity can aid in lowering excessive ROS, which can lessen cell damage from oxidative stress. This helps not only in the initial

https://doi.org/10.2147/IJN.S522589

inflammatory phase but also in the subsequent stages of proliferation and remodeling.[39] Therefore, the antioxidant activity of GC/OCS-CL@Cur was evaluated using DPPH and ABTS free radical scavenging. As shown in Figure 4e–h, the DPPH and ABTS free radical scavenging ratios of the CSLA@Cur and GC/OCS-CL@Cur groups were noticeably higher than those of the GelMA-CPBA, OCS, and GC/OCS groups. This suggests that CSLA@Cur and GC/OCS-CL @Cur exhibited exceptional antioxidant capabilities. However, the free radical scavenging ratio of GC/OCS-CL@Cur was slightly lower than that of CSLA@Cur. This may be because LA, as a natural antioxidant, fully exerts its antioxidant activity in the outer shell of the nano micelle.[40] However, since the active site was covered by hydrogel, the antioxidant activity of GC/OCS-CL@Cur was decreased. In the healing process of wounds, blood compatibility is crucial for medical dressings. Excellent blood compatibility can reduce complications and create a favorable healing environment for the wound.[41] The blood compatibility of GC/OCS-CL@Cur was evaluated by a hemolysis test, and the results are shown in Figure 4i. The hemolysis ratio of each group of hydrogels and drug-carrying nano micelles was lower than 0.17%, which belonged to the normal range, indicating that no hemolysis occurred. This demonstrates that GC/OCS-CL@Cur and other materials can be utilized as a very safe wound dressing and have great blood compatibility.

Biocompatibility of Hydrogels

Cytotoxicity is a key index to evaluate the safety of wound dressings. For 1 d, 3 d, and 5 d, cells were co-cultured with GC/OCS, CSLA@Cur, and GC/OCS-CL@Cur hydrogels. To assess cell viability, the cells were then exposed to live and dead staining and the CCK-8 assay. According to fluorescence imaging, cells in the GC/OCS, CSLA@Cur, and GC/OCS-CL@Cur groups all displayed a trend of continuous proliferation and retained their characteristic spindle shape within 5 d, as seen in Figure 5a. However, compared to the other groups, the GC/OCS-CL@Cur group exhibited a noticeably greater quantity of live cells. Additionally, there was no appreciable difference between the GC/OCS, CSLA@Cur, and GC/OCS-CL@Cur groups and the control group, and the GC/OCS, CSLA@Cur, and GC/OCS groups showed fewer dead cells as shown by red fluorescence. The CCK-8 experiment's findings demonstrated that GC/OCS-CL @Cur's cell activity was above 108%, which was marginally greater than that of the other groups (Figure 5c). The cell proliferation capacity of GC/OCS-CL@Cur hydrogel was further evaluated by crystal violet staining. Figure 5b shows that there were substantially more cells in the GC/OCS-CL@Cur group than in the other groups. The GC/OCS-CL@Cur group's cell proliferation ratio was 33.46% greater than the control groups, according to quantitative measurement of the cell proliferation ratio (Figure 5d). These results imply that GC/OCS-CL@Cur can significantly boost cell proliferation, which promotes the growth of new blood vessels and the regeneration of the epithelium of wound tissue.

In vitro Angiogenesis Analysis of Hydrogels

To visually observe the morphological changes of cells in wound tissue, cytoskeleton staining experiments were performed on cells co-cultured with various hydrogels (Figure 6a). As can be seen from the figure, cells cultured in the GC/OCS-CL@Cur group had a larger spread area, and showed clear elongated fusiform and clear pseudopods than those in the control group or GC/OCS, CSLA@Cur group. This suggests that GC/OCS-CL@Cur can keep cell structure and function in a better state. The capacity of cells to migrate and mend is essential for wound healing.[42] Thus, to assess the impact of hydrogels in each group on cell migration, cell scratch tests were conducted on cells co-cultured with GC/OCS, CSLA@Cur, and GC/OCS-CL@Cur (Figure 6b), and a quantitative study of cell mobility was carried out (Figure 6e). The figure shows that after 48 h, the mobility of the cells in the control group was 43.93% with only a modest migration phenomenon. Although the cell migration was obvious in GC/OCS and CSLA@Cur groups, the cell migration ratio was much lower than that in GC/OCS-CL@Cur group (82.27%). To further evaluate the cell invasion ability of hydrogels, Trans well cell invasion assay was performed on L929 cells and hydrogels, and the cells were fluorescently stained to visually observe the results. As shown in Figure 6c, cells in GC/OCS, CSLA@Cur, and GC/OCS-CL@Cur groups all had a certain invasion ability, but GC/OCS-CL@Cur group showed stronger fluorescence, indicating that GC/OCS-CL@Cur group had the largest number of successfully invaded cells. The control group had 86 cell migrations, but the GC/OCS, CSLA@Cur, and GC/OCS-CL@Cur groups all had cell migrations greater than 100, as shown by the quantitative statistical results of cell migration (Figure 6f). Furthermore, there were 182 cell migrations in

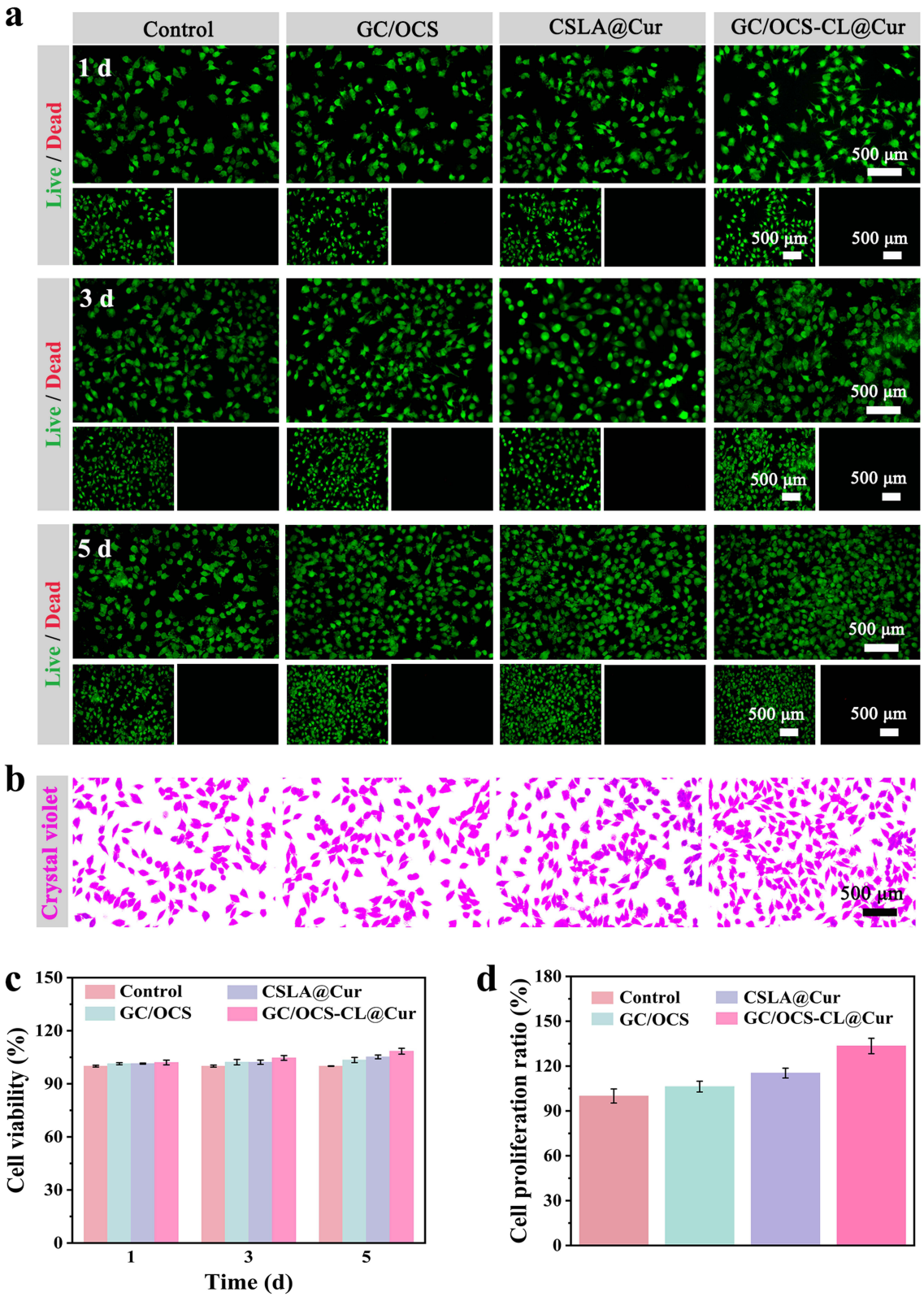

Figure 5 Cells were co-cultured with GC/OCS, CSLA@Cur, and GC/OCS-CL@Cur for 1 d, 3 d, and 5 d. (**a**) Fluorescent staining of live and dead cells and (**c**) quantitative statistics of CCK-8 cell viability. (**b**) Fluorescence images of crystal violet staining and (**d**) quantitative statistics of cell proliferation after co-culture with GC/OCS, CSLA@Cur, and GC/OCS-CL@Cur. n=5.

https://doi.org/10.2147/IJN.S522589

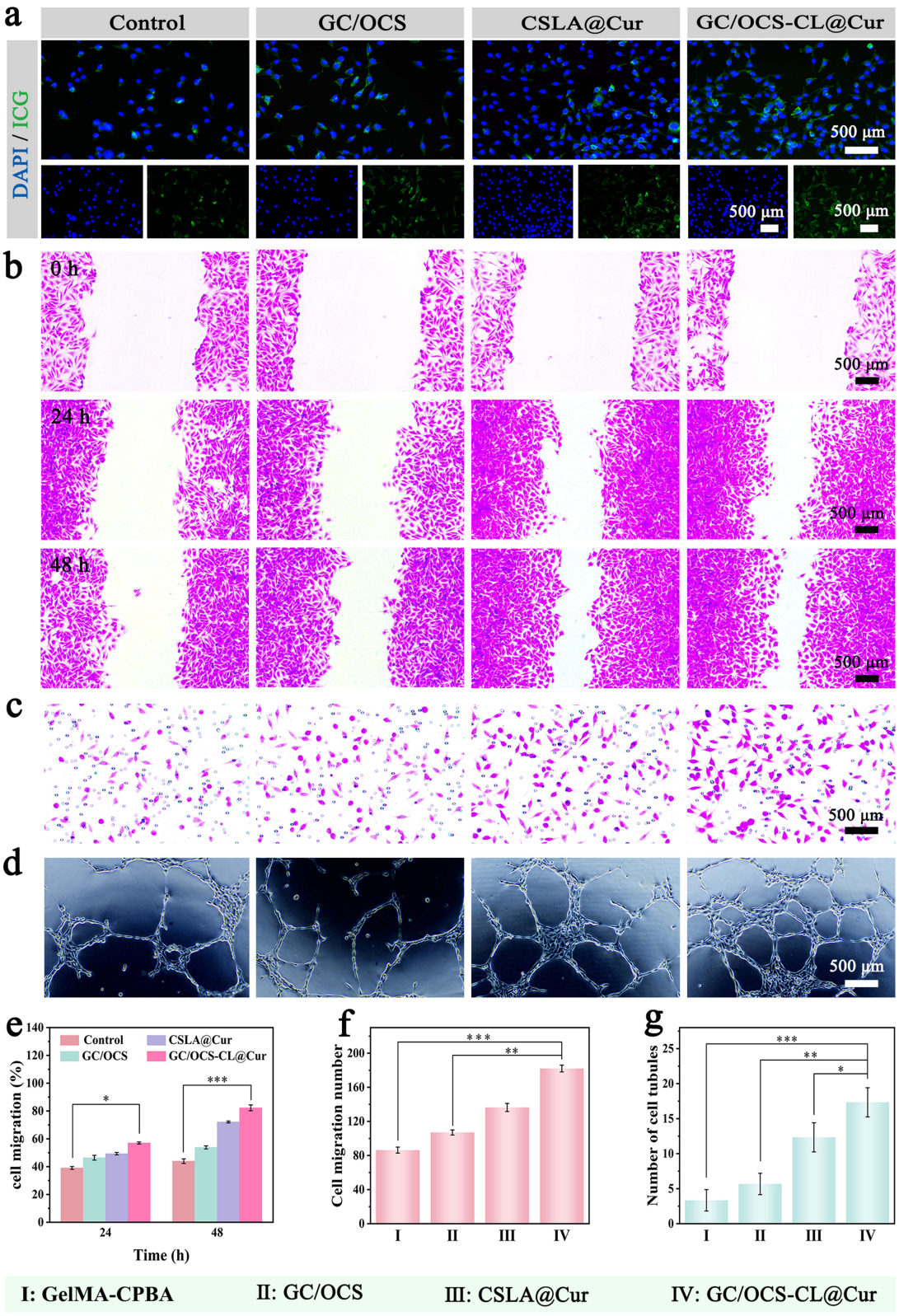

Figure 6 (**a**) Images of cytoskeleton fluorescence staining after co-culture with GC/OCS, CSLA@Cur, and GC/OCS-CL@Cur. (**b**) Cell scratch images and (**e**) quantitative statistics of cell mobility were obtained after 24 h and 48 h co-culture with GC/OCS, CSLA@Cur, and GC/OCS-CL@Cur. (**c**) Fluorescence staining images of trans well migration assay and (**f**) quantitative statistics of cell migration after co-culture with GC/OCS, CSLA@Cur, and GC/OCS-CL@Cur. (**d**) Images of cell tube forming experiment and (**g**) quantitative statistics of tube forming quantity after co-culture with GC/OCS, CSLA@Cur, and GC/OCS-CL@Cur. n=5. Significance levels of *p<0.055, **p<0.01, and ***p<0.001 were applied.

the GC/OCS-CL@Cur group, 2.12 times as many as in the control group. According to these findings, GC/OCS-CL @Cur can greatly increase cell invasion and, consequently, cell-to-cell contact.

Angiogenesis is a dynamic process that plays a critical role in wound healing. During the healing process, the generation of new blood vessels facilitates the transportation of blood, providing nutrients and oxygen to the wound. This, in turn, improves the oxygen supply to the wound and accelerates the healing process.[43] Moreover, the development of new blood vessels has been demonstrated to contribute to the production of granulation tissue, thereby facilitating wound healing.[44] Therefore, the effects of GC/OCS, CSLA@Cur, and GC/OCS-CL@Cur on angiogenesis of HUVEC cells in vitro were explored, and the results were shown in Figure 6d, and quantitative statistics were conducted on the number of new vessels (Figure 6g). The graphic shows that there are fewer annular structures and that the vascular network in the GC/OCS group still has deficiencies as compared to the control group. A full vascular network emerged and the cell coverage area grew in the CSLA@Cur and GC/OCS-CL@Cur groups. In contrast to the CSLA@Cur group, the GC/OCS-CL@Cur group's blood vessel network featured more branching points and loops, and there were 30% more new blood vessels. These results indicate that GC/OCS-CL@Cur can effectively promote the growth of neovascularization.

Antioxidant and Macrophage Polarization of Hydrogels

In bacterial infected wounds, due to excessive oxidative stress response will generate a substantial number of free radicals, which will cause serious damage to cells and tissues, and ultimately hinder wound healing.[45] Therefore, after RAW264.7 cells were treated with H_2O_2, the antioxidant activity of GC/OCS-CL@Cur was evaluated by DCFH-DA staining, and the intracellular ROS levels were quantitatively calculated. The fluorescence intensity of cells treated with H_2O_2 was very bright, as seen in Figure 7a, but the fluorescence intensity of the GC/OCS, CSLA@Cur, and GC/OCS-CL @Cur groups was much lower. These results indicate that GC/OCS, CSLA@Cur, and GC/OCS-CL@Cur have excellent antioxidant activities. The GC/OCS-CL@Cur group, on the other hand, had a reduced ROS level (10.37%), which was comparable to that of the control group (4.27%), according to the quantitative statistical diagram of cell ROS levels (Figure 7c). The synergistic interaction between GC/OCS and CSLA@Cur, which has been shown to increase the hydrogel's antioxidant activity, could be the cause of this phenomena.

The immunological microenvironment during skin wound healing is predominantly influenced by macrophages, which are pivotal immune cells that regulate wound healing.[46] Pro-inflammatory M1 macrophages and anti-inflammatory M2 macrophages are the two primary subtypes of macrophages, a kind of immune system cells. During the process of normal wound healing, it is essential that the balance between these two types of macrophages remains stable However, in cases of recalcitrant wounds, a shift towards an overactive state of M1 macrophages, known as "hyperpolarization", has been observed.[47] As a result, hydrogels' function as wound dressings in encouraging macrophage polarization from M1 to M2 is crucial for wound healing. Following LPS and IFN-γ treatment, RAW264.7 cells were co-cultured with GC/ OCS, CSLA@Cur, and GC/OCS-CL@Cur. The effect of GC/OCS-CL@Cur on the polarization of macrophages was evaluated by iNOS and CD206 immunofluorescence staining. Results As shown in Figure 7b, LPS, and IFN-γ treated cells showed high iNOS fluorescence intensity, while CD206 showed low fluorescence intensity. The fluorescence intensity of iNOS in GC/OCS, CSLA@Cur, and GC/OCS-CL@Cur groups decreased gradually, while the fluorescence intensity of CD206 increased gradually. These results showed that GC/OCS, CSLA@Cur, and GC/OCS-CL@Cur might promote macrophage polarization from M1 to M2 to some extent. Quantitative statistics on the fluorescence intensity of iNOS and CD206 were conducted (Figure 7d). It can be seen that the fluorescence intensity of iNOS in the GC/OCS-CL @Cur group decreased by 31.39%, while that in the GC/OCS and CSLA@Cur group decreased by 18.26% and 23.12%, respectively. The GC/OCS-CL@Cur group had the highest fluorescence intensity of CD206, increasing by 47.40% in comparison to the control group. To improve wound healing, it can be stated that GC/OCS-CL@Cur has a greater effect on polarizing macrophages and efficiently regulating the immunological microenvironment of wounds.

Histological Evaluation

A model of a full skin defect infected by bacteria was created in order to assess GC/OCS-CL@Cur's capacity for wound healing. The animal testing procedure is outlined in Figure 8a. After 3, 7, 10, and 14 days of treatment, wound healing

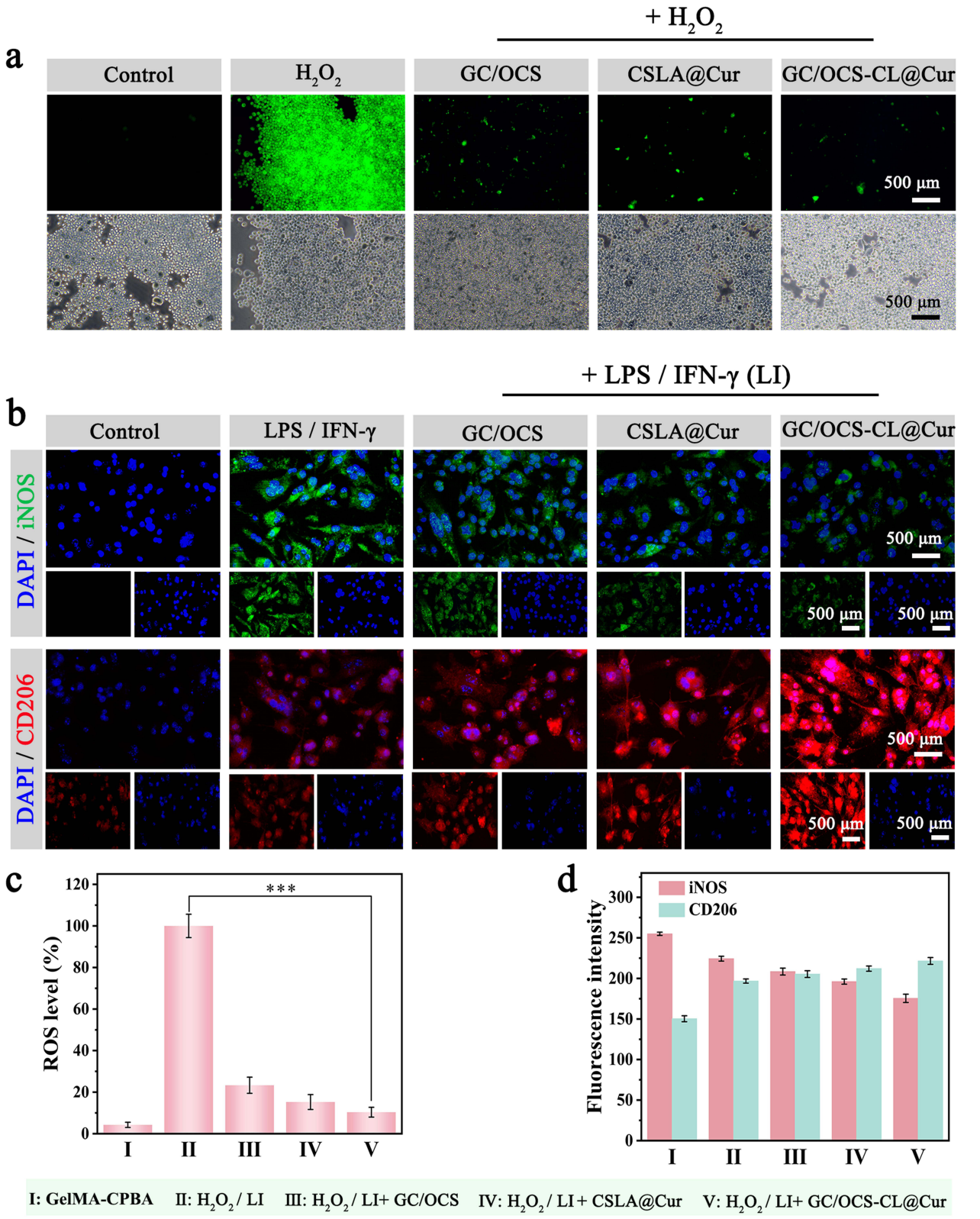

Figure 7 After co-culture with PBS, GC/OCS, CSLA@Cur, and GC/OCS-CL@Cur, cells treated with H_2O_2 were (**a**) DCFH-DA fluorescent staining images and (**c**) quantitative statistics of intracellular ROS levels. After the cells treated with LPS and IFN-γ were co-cultured with PBS, GC/OCS, CSLA@Cur, and GC/OCS-CL@Cur, (**b**) immunofluorescence staining images of iNOS and CD206 and (**d**) quantitative statistics of fluorescence intensity was obtained. n=5. Significance levels of ***$p<0.001$ were applied.

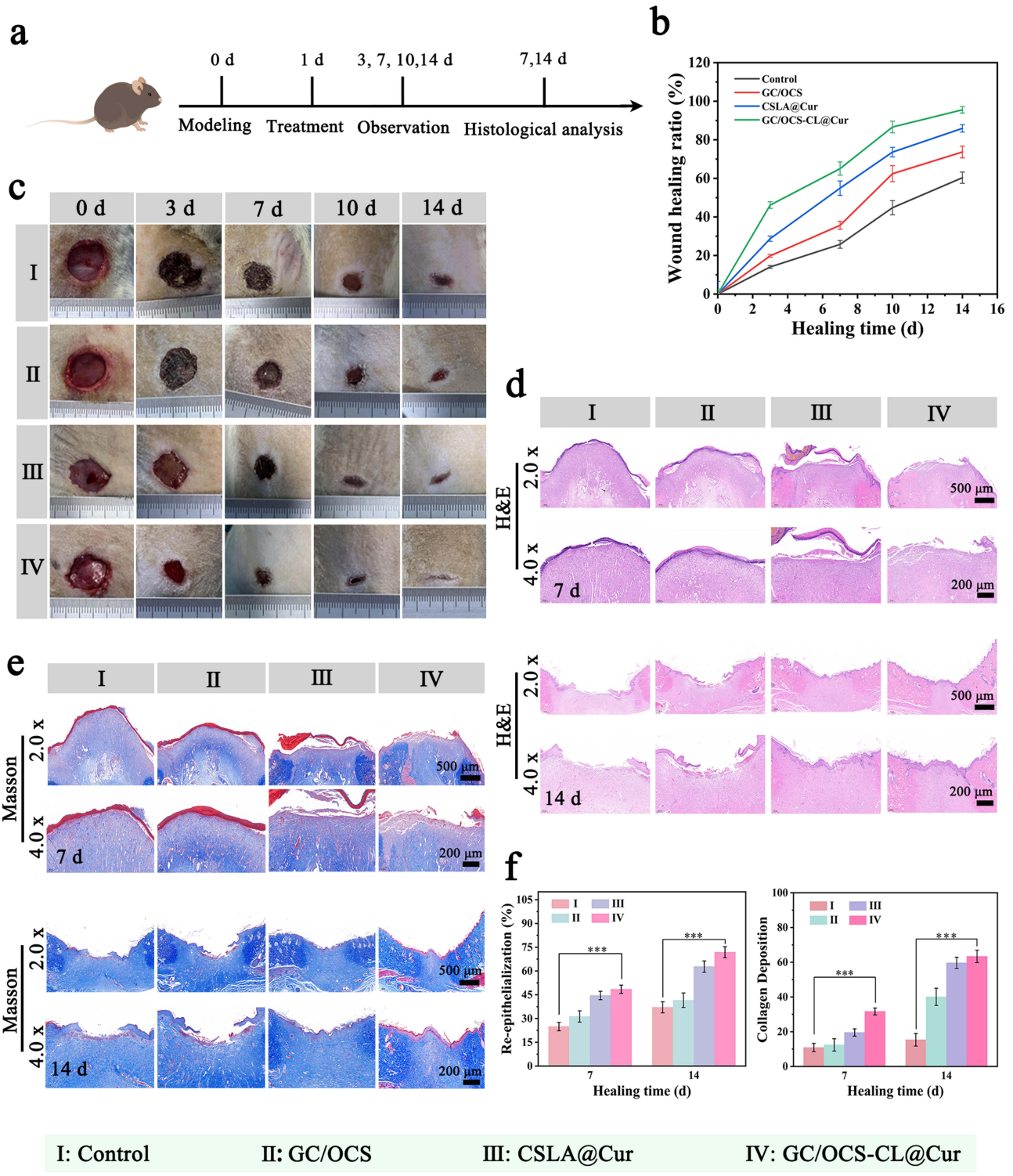

Figure 8 (**a**) Animal experimental process of bacterial infection wound healing. (**b**) Wound healing curves of GC/OCS, CSLA@Cur, and GC/OCS-CL@Cur for the treatment of bacterial infected wounds. (**c**) Digital photographs of healed wounds at 0 d,3 d, 7 d,10 d, 14 d. (**d**) H&E staining of wound healing tissue on day 7 and day 14. (**e**) Masson staining of wound healing tissue on day 7 and day 14. (**f**) Quantitative statistics of re-epithelialization ratio and collagen deposition in wound healing tissue at day 7 and day 14. n=6. Significance levels of ***p<0.001 were applied.

https://doi.org/10.2147/IJN.S522589

was monitored and recorded in each group using a digital camera, while wound healing curves were derived by calculating the wound area. As shown in Figure 8b and c, the groups receiving GC/OCS and CSLA@Cur demonstrated accelerated wound healing, with speeds of 35.65% and 54.93%, respectively, during the initial seven days of healing. Compared to the control groups, these ratios were noticeably greater. However, the wound healing ratio of the GC/OCS-CL@Cur group reached 46.14% at 3 d, and its wound healing speed was much higher than that of other groups. After that, it still leads the other groups with a super high healing speed. This may be because GC/OCS-CL@Cur combines the excellent swelling properties of GC/OCS with the diverse biological activities of CSLA@Cur, which results in faster wound healing. After 14 days, the wound was nearly fully healed and the GC/OCS-CL@Cur group's wound healing ratio had increased to 95.54%. This suggests that in bacterially infected areas, GC/OCS-CL@Cur can effectively promote wound healing.

Immunohistochemical analysis was done on the wound healing tissue after 7 and 14 d in order to see the morphological and structural changes that occur during the healing process. The ratio of collagen deposition to re-epithelialization in the healed tissue was assessed using H&E and Masson staining. According to the results of the H&E staining, the wound tissue of the GC/OCS group and the control group had modest hyperplasia on day 7 (Figure 8d). At this time, although there was no skin hyperplasia in the CSLA@Cur and GC/OCS-CL@Cur groups, the re-epithelialization was not significant. However, the arrangement of epithelial cells was not dense, and there was no discernible re-epithelialization on the 14 d, even though the hyperplasia of skin tissue had disappeared in the control group and GC/OCS group. On the other hand, the skin of CSLA@Cur and GC/OCS-CL@Cur groups showed an obvious upper cortex with an orderly arrangement of cells and distinct layers. Quantitative analysis of the staining results showed that the post-injury re-epithelialization ratio in the CSLA@Cur and GC/OCS-CL@Cur groups was 62.80% and 71.89%, respectively (Figure 8f). Furthermore, Masson staining results showed that on day 7, the GC/OCS and CSLA@Cur groups had noticeably greater levels of collagen and muscle fibers than the control group (Figure 8e). Despite the lack of evident alterations in muscle fibers, the GC/OCS-CL@Cur group had a higher proportion of collagen fibers and a denser organization. On the 14 d, collagen fibers in the GC/OCS-CL@Cur group were widely distributed, with clear layers and close arrangement. At the same time, there were significant muscle fiber layers, indicating that the skin tissue of the GC/OCS-CL@Cur group had good contractibility. However, compared to the CSLA@Cur and GC/OCS-CL@Cur groups, the GC/OCS group's collagen deposition and muscle fiber count were noticeably lower (Figure 8f). This phenomenon can be attributed to the lack of bioactivity in GC/OCS that promotes wound healing. And CSLA@Cur has significant antioxidant and anti-inflammatory properties, which help it effectively promote wound healing.

Anti-Inflammatory and Vascularization Properties of Hydrogels in vivo

In the initial phases of wound healing, a minor inflammatory reaction can facilitate the body's elimination of infections and damaged tissue. However, an excessively long-lasting inflammatory reaction can make inflammatory cells hyperactive and release a lot of inflammatory chemicals, which damages the tissue further and prevents wounds from healing.[48] Therefore, easing the excessive inflammatory response is crucial in the wound healing process. Immunohistochemical examination of IL-6 and IL-10 in wound healing tissue at day 7 was used to assess the function of GC/OCS-CL@Cur in controlling the inflammatory response. Findings The distribution density of IL-6 in the control group was quite high, as seen in Figure 9a, whereas it was lower in the GC/OCS, CSLA@Cur, and GC/OCS-CL@Cur groups. This suggests that they can, to some extent, lower the expression of inflammatory factors. However, the GC/OCS-CL@Cur group's IL-6 distribution density was noticeably lower than that of the control group. According to a quantitative examination of IL-6 relative expression, the GC/OCS-CL@Cur group's IL-6 relative expression was 25.63%, a 64.38% drop from the control group (Figure 9c). Furthermore, compared to the control group, the GC/OCS-CL@Cur group's IL-10 distribution density was significantly larger and its relative expression level rose 1.76 times. This indicates that GC/OCS-CL@Cur can significantly regulate the expression level of inflammatory factors, to effectively relieve excessive inflammatory response.

New blood vessel development can help the wound site receive oxygen and nutrients, which will aid in wound tissue regeneration and repair.[49] CD31, as a platelet endothelial cell adhesion molecule, contributes to wound hemostasis and angiogenesis.[50] α-SMA acts as smooth muscle actin, and its expression can promote wound contraction and collagen

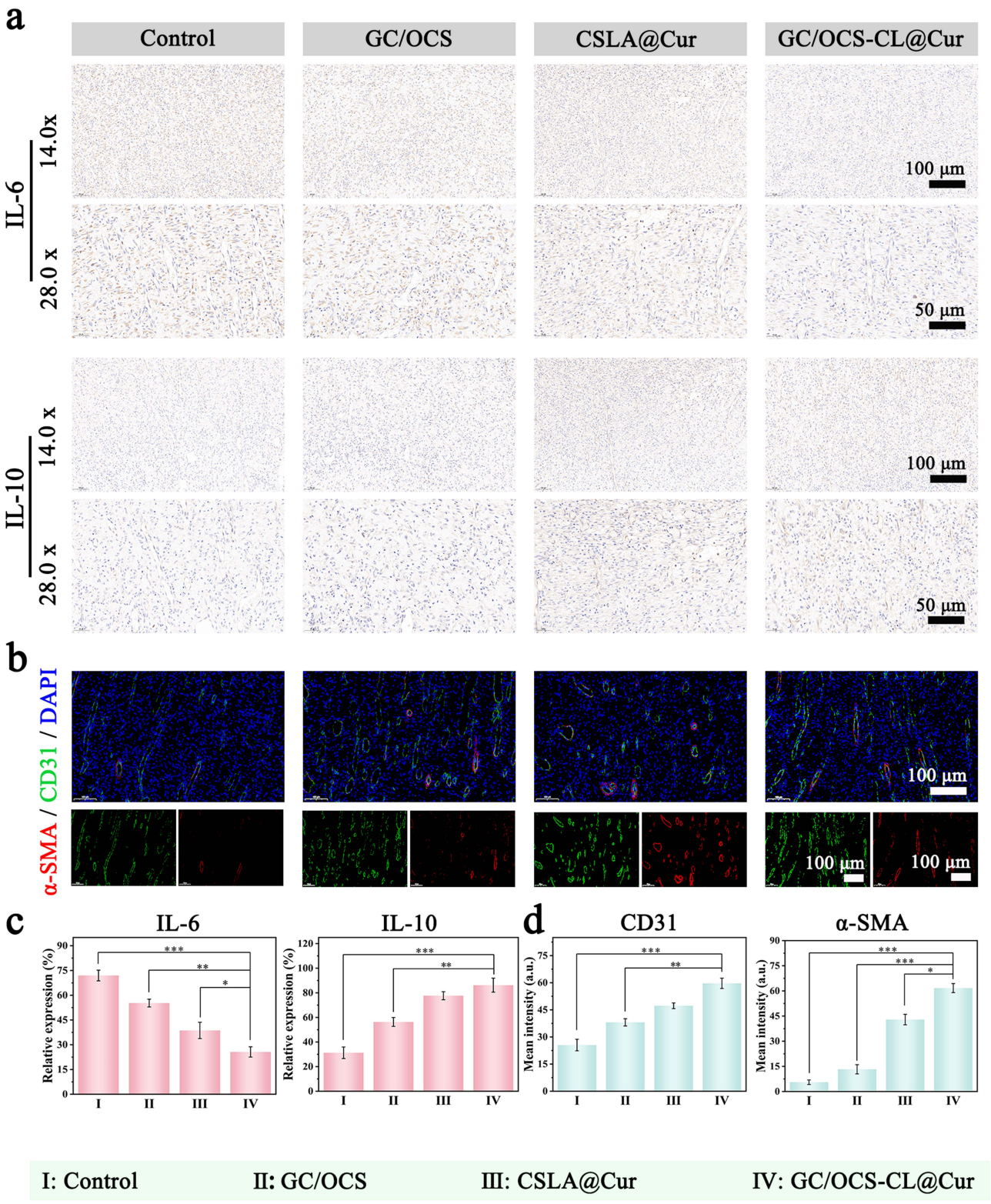

Figure 9 (**a**) immunohistochemical staining images of IL-6 and IL-10 and (**b**) immunofluorescence staining images of CD31 and α-SMA of the wound healed by PBS, GC/OCS, CSLA@Cur, and GC/OCS-CL@Cur. Quantitative statistics of (**c**) IL-6 and IL-10 expression levels and (**d**) CD31 and α-SMA fluorescence intensity in wound healing tissue. n=6. Significance levels of *p<0.055, **p<0.01, and ***p<0.001 were applied.

https://doi.org/10.2147/IJN.S522589

deposition.[51] In order to evaluate the neoangiogenic potential of GC/OCS-CL@Cur, immunofluorescence labeling for CD31 and α-SMA was carried out on wound healing tissues on day seven after trauma treatment. As seen in Figure 9b, the control group's CD31 and α-SMA fluorescence intensity was extremely low. Following treatment with GC/OCS, CSLA@Cur, and GC/OCS-CL@Cur, the fluorescence intensity progressively rose. Of these, the fluorescence intensity of CD31 and α-SMA in the GC/OCS-CL@Cur group was 1.34 and 0.69 times higher than in the control group, respectively (Figure 9d). These results suggest that by upregulating the expression of CD31 and α-SMA, GC/OCS-CL@Cur can encourage the neovascularization of wound tissue.

Conclusion

In conclusion, a ROS/pH dual-responsive hydrogel dressing (GC/OCS-CL@Cur) containing amphiphilic structured nano cellulose was successfully constructed for promoting bacterial infection wound healing. The nano micelles formed by chitosan-grafted ALA self-assembly were loaded with Cur and incorporated into a hydrogel matrix based on boronate ester bonds, Schiff base bonds, and free radical polymerization, thereby improving Cur's water solubility and achieving intelligent drug release. Due to the unique crosslinked structure, GC/OCS-CL@Cur exhibited excellent mechanical properties, appropriate swelling behavior, and sensitive ROS/pH dual-responsive properties. At high ROS levels and low pH environment, GC/OCS-CL@Cur exhibited significantly enhanced Cur release, reaching a release ratio of 68.75%, which was 66.30% higher than the drug release ratio under normal physiological conditions. Benefiting from ALA's outstanding antioxidant activity and Cur's potent anti-inflammatory and antioxidant bioactivities, GC/OCS-CL@Cur showed remarkable wound-healing efficacy. Free radical scavenging assay and antimicrobial assay showed that GC/OCS-CL@Cur could effectively scavenge free radicals and significantly inhibit bacterial growth. In vitro experiments demonstrated that GC/OCS-CL@Cur possessed excellent biocompatibility and was effective in promoting cell migration, facilitating tube formation of HUVECs, scavenging intracellular ROS and promoting macrophage polarization from M1-type to M2-type. In vivo experiments demonstrated that GC/OCS-CL@Cur significantly reduced inflammatory cytokine levels, promoted angiogenesis, and effectively accelerated wound healing, achieving a remarkable wound closure ratio of 95.54% within 14 days. Hence, this microenvironmentally responsive drug delivery system combining nano micelles with hydrogels offers a promising and innovative strategy for the management of bacterial infected wounds. To facilitate clinical translation, future studies should further investigate its mechanism in promoting infected wound repair and conduct clinical trials.

Acknowledgments

We gratefully acknowledge Guangzhou Myers Biotechnology Co., Ltd. for providing the experimental facilities and technical support for the animal studies in this research.

Funding

This work was supported by the Shenzhen Science and Technology Research and Development Fund (JCYJ20220530151608018); the Clinical Research Talent Project (NSZD2023048); the Basic Research Talent Project (NSZD2024058).

Disclosure

The authors declare no conflicts of interest in this work.

References

1. Hu W, Ouyang Q, Jiang C, et al. Biomedical metal–organic framework materials on antimicrobial therapy: perspectives and challenges. *Mater Today Chem*. 2024;41:102300. doi:10.1016/j.mtchem.2024.102300
2. Azul L, Leandro A, Boroumand P, Klip A, Seiça R, Sena CM. Increased inflammation, oxidative stress and a reduction in antioxidant defense enzymes in perivascular adipose tissue contribute to vascular dysfunction in type 2 diabetes. *Free Radical Bio Med*. 2020;146:264–274. doi:10.1016/j.freeradbiomed.2019.11.002
3. Cao Y, Jiang Y, Bai R, et al. A multifunctional protein-based hydrogel with Au nanozyme-mediated self generation of H2S for diabetic wound healing. *Int J Biol Macromol*. 2024;271:132560. doi:10.1016/j.ijbiomac.2024.132560

4. Liu Q, Luo S, Peng J, Chang R. Electrospun nanofibers from plant natural products: a new approach toward efficient wound healing. *Int J Nanomed*. 2024;19:13973–13990. doi:10.2147/IJN.S501970
5. Singh H, Hassan S, Nabi SU, et al. Multicomponent decellularized extracellular matrix of caprine small intestine submucosa based bioactive hydrogel promoting full-thickness burn wound healing in rabbits. *Int J Biol Macromol*. 2024;255:127810. doi:10.1016/j.ijbiomac.2023.127810
6. Wang X, Huang Y, Yang Y, et al. Polysaccharide-based biomaterials for regenerative therapy in intervertebral disc degeneration. *Mater Today Bio*. 2025;30:101395. doi:10.1016/j.mtbio.2024.101395
7. Yuan N, Shao K, Huang S, Chen C. Chitosan, alginate, hyaluronic acid and other novel multifunctional hydrogel dressings for wound healing: a review. *Int J Biol Macromol*. 2023;240:124321. doi:10.1016/j.ijbiomac.2023.124321
8. Sang F, Liu C, Yan J, et al. Polysaccharide- and protein-based hydrogel dressings that enhance wound healing: a review. *Int J Biol Macromol*. 2024;280:135482. doi:10.1016/j.ijbiomac.2024.135482
9. Cheng Y, Ling J, Ouyang X-K, Wang N. Curdlan/xanthan gum-based composite hydrogel with near-infrared irradiation responsive properties for infected wounds healing. *Int J Biol Macromol*. 2025;284:138199. doi:10.1016/j.ijbiomac.2024.138199
10. Fan L, Ge X, Qian Y, et al. Advances in synthesis and applications of self-healing hydrogels. *Front Bioeng Biotech*. 2020;8:654.
11. Deng X, Wu Y, Tang Y, et al. Microenvironment-responsive smart hydrogels with antibacterial activity and immune regulation for accelerating chronic wound healing. *J Control Release*. 2024;368:518–532. doi:10.1016/j.jconrel.2024.03.002
12. Wang P, Gong Q, Hu J, Li X, Zhang X. Reactive Oxygen Species (ROS)-responsive prodrugs, probes, and theranostic prodrugs: applications in the ROS-related diseases. *Eur J Med Chem*. 2021;64(1):298–325. doi:10.1021/acs.jmedchem.0c01704
13. Lee Y-M, Lu Z-W, Wu Y-C, Liao Y-J, Kuo C-Y. An injectable, chitosan-based hydrogel prepared by Schiff base reaction for anti-bacterial and sustained release applications. *Int J Biol Macromol*. 2024;269:131808. doi:10.1016/j.ijbiomac.2024.131808
14. Song F, Gong J, Tao Y, Cheng Y, Lu J, Wang H. A robust regenerated cellulose-based dual stimuli-responsive hydrogel as an intelligent switch for controlled drug delivery. *Int J Biol Macromol*. 2021;176:448–458. doi:10.1016/j.ijbiomac.2021.02.104
15. Qiao B, Wang J, Qiao L, Maleki A, Liang Y, Guo B. ROS-responsive hydrogels with spatiotemporally sequential delivery of antibacterial and anti-inflammatory drugs for the repair of MRSA-infected wounds. *Regen Biomater*. 2024;11:rbad110. doi:10.1093/rb/rbad110
16. Xie X, Lei H, Fan D. Antibacterial hydrogel with pH-responsive microcarriers of slow-release VEGF for bacterial infected wounds repair. *J Mater Sci Technol*. 2023;144:198–212. doi:10.1016/j.jmst.2022.09.062
17. He Y, Yang W, Zhang C, et al. ROS/pH dual responsive PRP-loaded multifunctional chitosan hydrogels with controlled release of growth factors for skin wound healing. *Int J Biol Macromol*. 2024;258:128962. doi:10.1016/j.ijbiomac.2023.128962
18. Zhang T, Guo L, Li R, et al. Ellagic acid–cyclodextrin inclusion complex-loaded thiol–ene hydrogel with antioxidant, antibacterial, and anti-inflammatory properties for wound healing. *ACS Appl. Mater. Interfaces*. 2023;15(4):4959–4972. doi:10.1021/acsami.2c20229
19. Ni S, Zhang K, Zhao X, et al. Phenylboronic acid functionalized dextran loading curcumin as nano-therapeutics for promoting the bacteria-infected diabetic wound healing. *Int J Biol Macromol*. 2024;273:133062. doi:10.1016/j.ijbiomac.2024.133062
20. Umerska A, Gaucher C, Oyarzun-Ampuero F, et al. Polymeric nanoparticles for increasing oral bioavailability of curcumin. *Antioxidants*. 2018;7(4):46. doi:10.3390/antiox7040046
21. Xue H, Ju Y, Ye X, Dai M, Tang C, Liu L. Construction of intelligent drug delivery system based on polysaccharide-derived polymer micelles: a review. *Int J Biol Macromol*. 2024;254:128048. doi:10.1016/j.ijbiomac.2023.128048
22. Yang X, Huang C, Wang H, et al. Multifunctional nanoparticle-loaded injectable alginate hydrogels with deep tumor penetration for enhanced chemo-immunotherapy of cancer. *ACS Nano*. 2024;18(28):18604–18621. doi:10.1021/acsnano.4c04766
23. Zhao Q, Liu J, Liu S, et al. Multipronged micelles–hydrogel for targeted and prolonged drug delivery in chronic wound infections. *ACS Appl. Mater. Interfaces*. 2022;14(41):46224–46238. doi:10.1021/acsami.2c12530
24. Hu C, Zhang F, Long L, Kong Q, Luo R, Wang Y. Dual-responsive injectable hydrogels encapsulating drug-loaded micelles for on-demand antimicrobial activity and accelerated wound healing. *J Control Release*. 2020;324:204–217. doi:10.1016/j.jconrel.2020.05.010
25. Bhadran A, Polara H, Calubaquib EL, et al. Reversible cross-linked thermoresponsive polycaprolactone micelles for enhanced stability and controlled release. *Biomacromolecules*. 2023;24(12):5823–5835. doi:10.1021/acs.biomac.3c00832
26. Tschiche A, Thota BNS, Neumann F, Schäfer A, Ma N, Haag R. Crosslinked redox-responsive micelles based on lipoic acid-derived amphiphiles for enhanced siRNA delivery. *Macromol Biosci*. 2016;16(6):811–823. doi:10.1002/mabi.201500363
27. Yuan Y, Wang Z, Su S, et al. Redox-sensitive self-assembled micelles based on low molecular weight chitosan-lipoic acid conjugates for the delivery of doxorubicin: effect of substitution degree of lipoic acid. *Int J Biol Macromol*. 2023;247:125849. doi:10.1016/j.ijbiomac.2023.125849
28. Shen F, Zhong H, Ge W, Ren J, Wang X. Quercetin/chitosan-graft-alpha lipoic acid micelles: a versatile antioxidant water dispersion with high stability. *Carbohydr Polym*. 2020;234:115927. doi:10.1016/j.carbpol.2020.115927
29. Zhou L, Dai C, Fan L, et al. Injectable self-healing natural biopolymer-based hydrogel adhesive with thermoresponsive reversible adhesion for minimally invasive surgery. *Adv Funct Mater*. 2021;31(14):2007457. doi:10.1002/adfm.202007457
30. Liu S, Zhao Y, Li M, et al. Bioactive wound dressing based on decellularized tendon and GelMA with incorporation of PDA-loaded asiaticoside nanoparticles for scarless wound healing. *Chem Eng J*. 2023;466:143016. doi:10.1016/j.cej.2023.143016
31. Martinelli M, Calderón M, Alvarez ICI, Strumia MC. Functionalised supports with sugar dendritic ligand. *React Funct Polym*. 2007;67(10):1018–1026. doi:10.1016/j.reactfunctpolym.2007.06.005
32. Bao Y, Cui H, Tian J, et al. Novel pH sensitivity and colorimetry-enhanced anthocyanin indicator films by chondroitin sulfate co-pigmentation for shrimp freshness monitoring. *Food Control*. 2022;131:108441. doi:10.1016/j.foodcont.2021.108441
33. Ashames A, Pervaiz F, Al-Tabakha M, et al. Synthesis of cross-linked carboxymethyl cellulose and poly (2-acrylamido-2-methylpropane sulfonic acid) hydrogel for sustained drug release optimized by Box-Behnken design. *J Saudi Chem Soc*. 2022;26(6):101541. doi:10.1016/j.jscs.2022.101541
34. Li D, Fei X, Wang K, et al. A novel self-healing triple physical cross-linked hydrogel for antibacterial dressing. *J Mater Chem B*. 2021;9(34):6844–6855. doi:10.1039/D1TB01257F
35. Feng W, Wang Z. Tailoring the Swelling-Shrinkable Behavior of Hydrogels for Biomedical Applications. *Adv Sci*. 2023;10(28):2303326. doi:10.1002/advs.202303326
36. Pan G, Li M, Mu L, Huang Y, Liang Y, Guo B. Photothermal/photodynamic synergistic antibacterial hydrogel dressing with pH/glucose dual responsive pirfenidone release for diabetic foot ulcers. *Adv Funct Mater*. 2024;35:2416205.

37. Zhang J, Shi X, Zhao Z, Wang M, Deng H, Du Y. Hydrogel films with impact resistance by sacrificial micelle-assisted-alignment. *Adv Sci*. 2024;11(44):2409287. doi:10.1002/advs.202409287
38. Zheng Y, Wang M, Zhang X, Wu Z, Gao L. A bacteria-responsive nanoplatform with biofilm dispersion and ROS scavenging for the healing of infected diabetic wounds. *Acta Biomater*. 2024;2024;1.
39. Pranantyo D, Yeo CK, Wu Y, et al. Hydrogel dressings with intrinsic antibiofilm and antioxidative dual functionalities accelerate infected diabetic wound healing. *Nat Commun*. 2024;15(1):954. doi:10.1038/s41467-024-44968-y
40. Tan E, Wan T, Pan Q, et al. Dual-responsive nanocarriers for efficient cytosolic protein delivery and CRISPR-Cas9 gene therapy of inflammatory skin disorders. *Sci Adv*. 2024;10(16):eadl4336. doi:10.1126/sciadv.adl4336
41. Zhou Q, Luo L, Zhou Z, et al. Low-temperature plasma-treated polyethylene oxide for hemostasis and skin wound healing. *Eur Polym J*. 2024;217:113268. doi:10.1016/j.eurpolymj.2024.113268
42. Ma C, Li Y, Liu B, et al. Exosomes derived from adipose mesenchymal stem cells promote corneal injury repair and inhibit the formation of scars by anti-apoptosis. *Colloids Surf B Biointerfaces*. 2025;247:114454. doi:10.1016/j.colsurfb.2024.114454
43. Sun Y, Zhang S, Shen Y, et al. Therapeutic application of mesenchymal stem cell-derived exosomes in skin wound healing. *Front Bioeng Biotech*. 2024;12:1428793.
44. Rodrigues M, Kosaric N, Bonham CA, Gurtner GC. Wound healing: a cellular perspective. *Physiol Rev*. 2018;99(1):665–706. doi:10.1152/physrev.00067.2017
45. Hayes JD, Dinkova-Kostova AT, Tew KD. Oxidative stress in cancer. *Cancer Cell*. 2020;38(2):167–197. doi:10.1016/j.ccell.2020.06.001
46. Su X, Yang J, Xu Z, et al. Fibrous scaffolds loaded with BMSC-derived apoptotic vesicles promote wound healing by inducing macrophage polarization. *Genes Dis*. 2025;12(2):101388. doi:10.1016/j.gendis.2024.101388
47. Zhang T, Tai Z, Miao F, et al. Bioinspired nanovesicles derived from macrophage accelerate wound healing by promoting angiogenesis and collagen deposition. *J Mater Chem B*. 2024;12(47):12338–12348. doi:10.1039/D3TB02158K
48. Cooke JP, Lai L. Transflammation in tissue regeneration and response to injury: how cell-autonomous inflammatory signaling mediates cell plasticity. *Adv Drug Deliv Rev*. 2023;203:115118. doi:10.1016/j.addr.2023.115118
49. Li W, Liu Y-H, Kubo F, Werner S, Razansky D. Skin layer-specific spatiotemporal assessment of micrometabolism during wound angiogenesis. *Commun Biol*. 2024;7(1):1574. doi:10.1038/s42003-024-07257-4
50. Wang Y, luo M, Li T, Xie C, Li S, Lei B. Multi-layer-structured bioactive glass nanopowder for multistage-stimulated hemostasis and wound repair. *Bioact Mater*. 2023;25:319–332. doi:10.1016/j.bioactmat.2023.01.019
51. Zhang G, Zhang Z, Cao G, et al. Engineered dermis loaded with confining forces promotes full-thickness wound healing by enhancing vascularisation and epithelialisation. *Acta Biomater*. 2023;170:464–478. doi:10.1016/j.actbio.2023.08.049